JOURNAL OF BACTERIOLOGY, May 2009, p. 3024–3040 Vol. 191, No. 9
0021-9193/09/$08.00+0 doi:10.1128/JB.01505-08

Influences of Capsule on Cell Shape and Chain Formation of Wild-Type and *pcsB* Mutants of Serotype 2 *Streptococcus pneumoniae*▽†

Skye M. Barendt,[1] Adrian D. Land,[1] Lok-To Sham,[1] Wai-Leung Ng,[1]‡ Ho-Ching T. Tsui,[1] Randy J. Arnold,[2] and Malcolm E. Winkler[1]*

Department of Biology[1] and Department of Chemistry,[2] Indiana University Bloomington, Bloomington, Indiana 47405

Received 24 October 2008/Accepted 20 February 2009

PcsB is a protein of unknown function that plays a critical role in cell division in *Streptococcus pneumoniae* and other ovococcus species of *Streptococcus*. We constructed isogenic sets of mutants expressing different amounts of PcsB in laboratory strain R6 and virulent serotype 2 strain D39 to evaluate its cellular roles. Insertion mutagenesis in parent and *pcsB*$^+$ merodiploid strains indicated that *pcsB* is essential in serotype 2 *S. pneumoniae*. Quantitative Western blotting of wild-type and epitope-tagged PcsB showed that all PcsB was processed into cell-associated and secreted forms of the same molecular mass and that cell-associated PcsB was moderately abundant and present at ≈4,900 monomers per cell. Controlled expression and complementation experiments indicated that there was a causative relationship between the severity of defects in cell division and decreasing PcsB amount. These experiments also showed that perturbations of expression of the upstream *mreCD* genes did not contribute to the cell division defects of *pcsB* mutants and that *mreCD* could be deleted. Unexpectedly, capsule influenced the cell shape and chain formation phenotypes of the wild-type D39 strain and mutants underexpressing PcsB or deleted for other genes involved in peptidoglycan biosynthesis, such as *dacA*. Underexpression of PcsB did not result in changes in the amounts or composition of lactoyl-peptides, which were markedly different in the R6 and D39 strains, and there was no correlation between decreased PcsB amount and sensitivity to penicillin. Finally, microarray analyses indicated that underexpression of PcsB may generate a signal that increases expression of the VicRK regulon, which includes *pcsB*.

Comparatively little is known about the exact mechanisms and interactions that occur during peptidoglycan (PG) biosynthesis and cell division of ovococcus bacteria, such as *Streptococcus pneumoniae* (pneumococcus) and other *Streptococcus* species (reviewed recently in reference 71). These ovoid, football-shaped bacteria divide along successive parallel planes perpendicular to the long axis of the cell. This mode of division contrasts with that of spherical coccus species such as *Staphylococcus aureus*, which divides in alternating perpendicular planes. Another major difference between these two bacterial types is that ovococcus species have two modes of PG biosynthesis (peripheral and septal), whereas spherical species have only septal PG biosynthesis (30, 38, 50, 51, 71). All models of PG biosynthesis require murein hydrolases, such as amidases or endopeptidases, to participate in PG remodeling and cell separation during division (15, 48, 66, 67, 71).

One candidate murein hydrolase is the PcsB protein, which has been characterized to various degrees in *S. pneumoniae* (29, 42, 45, 46), *Streptococcus mutans* (where it is called GbpB) (11, 12, 40, 41), and *Streptococcus agalactiae* (55, 56). PcsB orthologs contain four domains: a signal peptide (SP) that directs export, a predicted extended coiled-coil domain that contains leucine zipper motifs, an alanine-rich linker region that is variable in different *Streptococcus* species, and a CHAP (Cys, His-dependent amidohydrolase/peptidase) domain, which contains a conserved Cys292, His343, and Asn366 catalytic triad (1, 3, 35). CHAP domain proteins, such as Sle1 from *Staphylococcus aureus* and some bacteriophage hydrolases, function as *N*-acetylmuramyl-L-alanine amidases (i.e., they cleave the amide bond between *N*-acetyl-muramic acid in the glycan chain and L-Ala in stem peptides [16, 32, 54, 67]). The Sle1 amidase is not a homolog of PcsB, because its N-terminal domain contains a LysM PG binding motif instead of a coiled-coil domain (32). In addition, purified Sle1 amidase shows robust hydrolase activity in different assay formats at physiological pH (≈7.0) (32), whereas purified pneumococcal PcsB and its orthologs have failed to show murein hydrolase activity so far (see Discussion) (29, 41, 55, 56, 67).

Moderate underexpression of pneumococcal PcsB in unencapsulated laboratory strain R6 caused formation of medium-length chains containing slightly distorted, compressed cells (see Results) (45), and depletion of PcsB in unencapsulated and encapsulated isolates of different pneumococcal serotypes caused severe morphological and growth defects (29, 45). Similar to its GbpB orthologs in *S. mutans* and *S. agalactiae* (11, 40, 56), a considerable amount of pneumococcal PcsB is secreted into the growth medium (see Results) (29, 42, 45), and

* Corresponding author. Mailing address: Department of Biology, Indiana University Bloomington, Jordan Hall, Room 142, Bloomington, IN 47405. Phone: (812) 856-1318. Fax: (812) 855-6705. E-mail: mwinkler@bio.indiana.edu.

† Supplemental material for this article may be found at http://jb.asm.org/.

‡ Present address: 322 Lewis Thomas Lab, Princeton University, Washington Rd., Princeton, NJ 08544.

▽ Published ahead of print on 6 March 2009.

genomic fingerprinting of human antibodies collected from patients exposed to *S. pneumoniae* identified PcsB as a leading candidate for the development of a protein-based vaccine (29). Transcription of the *pcsB* gene is positively regulated by the essential VicRK two-component regulatory system, which has orthologs (called YycFG or WalRK) in all low-GC gram-positive species (18, 46, 47, 68). In fact, the apparent essentiality of the VicR response regulator is due to its positive regulation of *pcsB* in *S. pneumoniae* (46). In *Bacillus subtilis* and *S. aureus*, the YycFG (WalRK) regulons contain several known murein hydrolases (8, 17, 31), and it has been proposed that the YycFG (WalRK) and VicRK two-component systems function to maintain cell wall and cell surface homeostasis (18, 68).

Certain results reported for pneumococcal PcsB and its orthologs seem contradictory. Some reports claim that PcsB orthologs are essential (41, 45, 62), whereas others have found PcsB nonessential (11, 29, 55). A recent paper suggested that cell-associated pneumococcal PcsB is largely unprocessed and still contains its signal peptide (42), whereas two forms were not reported previously for PcsB from other species (40, 56). PcsB orthologs have been reported to localize to the cell wall (41) as well as to the cell membrane (42). Cochromatography, coimmunoprecipitation, and two-hybrid approaches have suggested that PcsB orthologs have the potential to interact with various proteins, including EF-Ts, ribosomal protein L7/L12, and DivIVA (21, 41), which are predominantly cytoplasmic.

In this study, we report the characterization of sets of isogenic mutants constructed in pneumococcus laboratory strain R6 and virulent serotype 2 strain D39 expressing different amounts of PcsB. We used these strains to provide new information about some of the properties mentioned above for which there are contradictory results. We demonstrate that the cell division and shape phenotypes of *pcsB* mutants are due to underexpression of PcsB and not perturbation of the expression of the upstream *mreCD* genes, which are dispensable in strains R6 and D39. In addition, we report unexpected links between cell shape and chain formation phenotypes and the presence of capsule. However, we did not detect a correlation between decreased PcsB or absence of MreCD and the composition of peptides in PG or sensitivity to penicillin. These results are discussed in terms of possible functions of PcsB in PG biosynthesis and signaling.

MATERIALS AND METHODS

Bacterial strains and growth conditions. Strains used in this study are listed in Table 1. Bacteria were grown on plates containing trypticase soy agar II (modified; Becton-Dickinson) and 5% (vol/vol) defibrinated sheep blood (TSAII BA) and incubated at 37°C in an atmosphere of 5% CO_2. Strains were also cultured statically in Becton-Dickinson brain heart infusion (BHI) broth (or in one case, chemically defined medium [CDM] [47]) at 37°C in an atmosphere of 5% CO_2, and growth was monitored by optical density at 620 nm (OD_{620}) using a Spectronic 20 spectrophotometer fitted for measurement of capped tubes (outer diameter, 16 mm). Bacteria were inoculated into BHI broth from frozen cultures or colonies, serially diluted into the same medium, and propagated overnight. Overnight cultures that were still in exponential phase (OD_{620}, 0.2 to 0.6) were diluted back to an OD_{620} of ≈0.005 to start final cultures, which did not contain antibiotics, except for strains containing plasmids, for which erythromycin was added to 0.3 μg per ml. For depletion of PcsB, cultures were first grown to exponential phase in BHI broth containing L-fucose (0.2% to 1.2% [wt/vol] as indicated). Cells were then collected by centrifugation for 10 min (3,200 × *g*; 25°C), washed twice with BHI broth lacking L-fucose, resuspended in the starting volume of BHI broth, and incubated for 5 h at 37°C.

Construction and verification of *S. pneumoniae* mutants. Strains containing antibiotic markers were constructed by transforming linear DNA amplicons synthesized by overlapping fusion PCR into competent pneumococcal cells as described previously (46, 57). Primers synthesized for this study are listed in Table S1 of the supplemental material. Transformations were carried out as described before (46, 57), except that incubations containing synthetic competence stimulatory peptide 1 (CSP-1) were shortened from 13 min to 10 min. TSAII BA plates were supplemented as appropriate with the following final concentrations of antibiotics: 250 μg kanamycin per ml, 100 μg spectinomycin per ml, 150 μg streptomycin per ml, or 0.3 μg erythromycin per ml. All constructs were confirmed by DNA sequencing of genomic DNA, which was prepared from cell lysates (5 μl of culture plus 30 μl of 1× PCR buffer; heated for 10 min at 95°C) and amplified using *Pfu* Turbo polymerase (Stratagene) or r*Tth* polymerase (Applied Biosystems). Amplicons were purified using a PCR cleanup kit (Qiagen) and sequenced in reaction mixtures containing 1 μl of Big Dye Terminator reagent (Applied Biosystems) as described previously (33). Sequences were aligned and analyzed using Vector NTI software (Invitrogen).

Construction of plasmid expressing PcsB. pLS1RGFP (65) was propagated in *Lactococcus lactis* NZ9000 in order to preserve the XhoI restriction sites. For cloning and expression, the $pcsB^+$ gene was amplified by PCR from *S. pneumoniae* R6 genomic DNA using forward primer SC133 and reverse primer SC134 (see Table S1 in the supplemental material), both having XhoI cut sites in their 5′ ends. The amplicon was digested with XhoI, ligated to XhoI-digested pLS1RGFP DNA, and transformed into *S. pneumoniae* strain R6 (EL59) (Table 1). The resulting pLSR1GFP::P_{mal}-$pcsB^+$ plasmid was purified using a miniprep procedure (Qiagen), modified by the addition of 1 mg lysozyme per ml and 50 mM sterile glucose to suspended cell pellets. Restriction analysis and DNA sequencing were used to verify the insert in plasmid pLSR1GFP::P_{mal}-$pcsB^+$, which expressed PcsB under the control of a maltose-inducible promoter.

Purification of PcsB-(C)-His_6 and production of purified antibody. PcsB-(C)-His_6 lacking the 27-amino-acid signal peptide was overexpressed in *E. coli* BL21(DE3) cells (Invitrogen) from plasmid pET22b::*pcsB′*, which was constructed by conventional methods using the primers listed in Table S1 of the supplemental material containing added NdeI and XhoI restriction sites. A 3-liter culture was grown in LB broth containing 100 μg ampicillin per ml at 30°C to an OD_{620} of ≈0.4 and induced by the addition of 1 mM 5-bromo-4-chloro-3-indolyl-β-D-thiogalactopyranoside (IPTG) for 3 h. Cells were collected by centrifugation for 20 min (4,400 × *g*; 4°C), resuspended in 20 mM $NaPO_4$, pH 7.0, 0.5 M NaCl, 10 mM imidazole, 1 mM β-mercaptoethanol (buffer A), and disrupted by passage through a French pressure cell twice. Cell debris was removed by centrifugation for 20 min (23,300 × *g*; 4°C), and the supernatant was filtered through an Acrodisc 0.22-μm Supor filter (Pall Scientific) before loading onto a Hi-Trap chelating column (Amersham) charged with Ni^{+2} according to the manufacturer's instructions. PcsB-(C)-His_6 was eluted by a 10 to 300 mM imidazole gradient in buffer A that was monitored by sodium dodecyl sulfate-polyacrylamide gel electrophoresis (SDS-PAGE). Fractions containing PcsB-(C)-His_6 were pooled and concentrated fourfold during buffer exchange to 100 mM $NaPO_4$, pH 7.4, 2 mM dithiothreitol using a 15 ml Centricon filter (10-kDa cutoff; Amicon). The buffer was exchanged again to 20 mM Tris-HCl, pH 8.0, and the sample was loaded onto a MonoQ column (10 mm by 100 mm; Amersham). PcsB-(C)-His_6 was eluted with a gradient of 0 to 1.0 M NaCl in 20 mM Tris-HCl, pH 8.0, and assayed by SDS-PAGE. Pooled factions were concentrated during buffer exchange to a final volume of 2.0 ml in phosphate-buffered saline (PBS; 137 mM NaCl, 10 mM $NaPO_4$, 2.7 mM KCl, pH 7.4), which contained 7.4 mg of PcsB-(C)-His_6 as determined by the nanodrop A_{280} or the DC protein assay (Bio-Rad) with bovine serum albumin (BSA) as the standard at >99% purity based on Coomassie-stained SDS-PAGE.

Polyclonal antibody was prepared against purified PcsB-(C)-His_6 in rabbits (Cocalico Biologicals). Anti-PcsB serum was purified using a nitrocellulose binding affinity method (52). Briefly, 300 μg of purified PcsB-(C)-His_6 was resolved by SDS-PAGE (see below) and transferred electrophoretically at 350 mA for 1 h to a nitrocellulose membrane (0.45 um; Osmonics, Inc.) in Towbin buffer (25 mM Trizma base, 192 mM glycine, 20% [vol/vol] methanol). The membrane was stained with 0.1% (wt/vol) Ponceau-S dye in 5% (vol/vol) acetic acid for 10 s and rinsed repeatedly with Tris-buffered saline with Tween 20 (TBS-T; 25 mM Tris-HCl, pH 7.4, 150 mM NaCl, 2 mM KCl, 0.1% [vol/vol] Tween 20) until the PcsB-(C)-His_6 protein band could be visualized. The nitrocellulose portion containing the purified protein was excised and blocked in 5% enhanced chemiluminescence (ECL) blocking reagent (Amersham) for 15 min at room temperature, incubated with 1 ml of anti-PcsB serum (saturated with 12 mg of BSA [Sigma]) for 4 h at room temperature, and eluted with 1 ml of Gentle Ag/Ab elution buffer (Pierce) for 15 min at room temperature. The eluate containing purified anti-PcsB antibody was dialyzed overnight at 4°C into TBS (25 mM

TABLE 1. Strains used in the study[a]

Strain	Genotype (derivation)	Antibiotic resistance[b]	Reference or source
EL59	Unencapsulated laboratory strain R6 derived from intermediates of strain D39	None	33
EL1454	R6 *kan*1t2-P_c-*pcsB*$^+$	Kan^r	46
IU1533	R6 Δ*bgaA′*::*kan*1t2-P_c-*pcsB*$^+$	Kan^r	45
IU1545	R6 *kan*1t2-P_{fcsK}-*pcsB*$^+$	Kan^r	45
IU1547	R6 Δ*pcsB*<>P_c-*ermAM* Δ*bgaA*<> *kan*1t2-P_c-*pcsB*	Erm^r Kan^r	45
IU1614	*E. coli* BL21(DE3) [pET22B::*pcsB*(ΔN27)]	Amp^r	This study
IU1621	R6 *kan*1t2-P_c-*pcsB*$^+$ Δ*bgaA′*::P_c-*aad9* (new amplicon × IU1454)	Kan^r Spec^r	This study
IU1690	Serotype 2 encapsulated D39 (NCTC 7466)	None	33
IU1705	R6 Δ*dacA*::P_c-*aad9* (new amplicon × EL59)	Spec^r	This study
IU1744	R6 *kan*1t2-P_c-*pcsB*$^+$ (amplicon from EL1454 × EL59)	Kan^r	This study and reference 45
IU1751	R6 Δ*mreCD*<>*aad9* (new amplicon × EL59)	Spec^r	This study
IU1781	D39 *rpsL1*	Str^r	53
IU1783	D39 *rpsL1* Δ*cps2BCDE*<>*kan-rpsL* (new amplicon × IU1781)	Str^r Kan^r	33
IU1807	D39 *kan*1t2-P_c-*pcsB*$^+$ (amplicon from EL1454 × IU1690)	Kan^r	This study
IU1845	R6 *pcsB*$^+$-FLAG P_c-*ermAM* (new amplicon × EL59)	Erm^r	This study
IU1859	*E. coli* BL21(DE3) [pET15B::*mreC*(ΔN32)]	Amp^r	This study
IU1945[c]	D39 Δ*cps*2A′ (*cps*2BCDETFG)H′	None	33
IU1979	R6 Δ*pcsB*<>*ermAM* Δ*bgaA′*::*kan*1t2-P_c-*pcsB*$^+$ (new amplicon × IU1533)	Erm^r Kan^r	This study
IU1983	R6 Δ*mreCD*<>*aad9* (amplicon from IU1751 × EL59)	Spec^r	This study
IU2091	D39 *kan*1t2-P_{fcsK}-*pcsB*$^+$ (amplicon from IU1545 × IU1690)	Kan^r	This study
IU2102	D39 Δ*mreCD*<>*aad9* (amplicon from IU1751 × IU1690)	Spec^r	This study
IU2105	D39 *pcsB*$^+$-FLAG P_c-*ermAM* (amplicon from IU1845 × IU1690)	Erm^r	This study
IU2142	*L. lactis* NZ9000 (pLS1RGFP) (plasmid × NZ9000)	Erm^r	65
IU2191	R6 (pLS1RGFP) (plasmid × EL59)	Erm^r	This study
IU2192	R6 (pLS1RGFP::P_{mal}-*pcsB*$^+$) (ligation mixture × EL59)	Erm^r	This study
IU2336	D39 Δ*cps*2A′ (*cps*2BCDETFG)H′ *kan*1t2-P_c-*pcsB*$^+$ (amplicon from IU1744 × IU1945)	Kan^r	This study
IU2517	D39 Δ*bgaA′*::*kan*1t2-P_c-*pcsB*$^+$ (amplicon from IU1533 × IU1690)	Kan^r	This study
IU2519	D39 Δ*bgaA′*::*kan*1t2-P_{fcsK}-*pcsB*$^+$ (new amplicon × IU1690)	Kan^r	This study
IU2537	D39 Δ*pcsB*<>*ermAM* Δ*bgaA′*::*kan*1t2-P_c-*pcsB*$^+$ (amplicon from IU1979 × IU2517)	Erm^r Kan^r	This study
IU2539	D39 Δ*pcsB*<>*ermAM* Δ*bgaA′*::*kan*1t2-P_{fcsK}-*pcsB*$^+$ (amplicon from IU1979 × IU2519)	Erm^r Kan^r	This study
IU2547	D39 Δ*bgaA′*::P_c-*aad9* (amplicon from IU1621 × IU1690)	Spec^r	This study
IU2551	D39 Δ*cps*2A′ (*cps*2BCDETFG)H′ *kan*1t2-P_c-*pcsB*$^+$ (pLS1RGFP::P_{mal}-*pcsB*$^+$) (plasmid from IU2192 × IU2336)	Kan^r Erm^r	This study
IU2564	R6 *kan*1t2-P_c-*pcsB*$^+$ (pLS1RGFP::P_{mal}-*pcsB*$^+$) (plasmid from IU2192 × IU1744)	Kan^r Erm^r	This study
IU2566	D39 Δ*cps*2A′ (*cps*2BCDETFG)H′ (pLS1RGFP::P_{mal}-*pcsB*$^+$) (plasmid from IU2192 × IU1945)	Erm^r	This study
IU2592	R6 Δ*bgaA′*::*kan*1t2-P_{fcsK}-*pcsB*$^+$ (amplicon from IU2519 × EL59)	Kan^r	This study
IU2604	D39 Δ*cps*2A′ (*cps*2BCDETFG)H′ (pLS1RGFP) (plasmid from IU2191 × IU1945)	Erm^r	This study
IU2608	R6 *kan*1t2-P_c-*pcsB*$^+$ (pLS1RGFP) (plasmid from IU2191 × IU1744)	Kan^r Erm^r	This study
IU2610	D39 Δ*cps*2A′ (*cps*2BCDETFG)H′ *kan*1t2-P_c-*pcsB*$^+$ (pLS1RGFP) (plasmid from IU2191 × IU2336)	Kan^r Erm^r	This study
IU2718	R6 Δ*bgaA′*::*erm*1t2-P_{fcsK}-*pcsB*$^+$ (A27D) (new amplicon x EL59)	Erm^r	This study
IU2801	R6 Δ*pcsB*<>*ermAM* Δ*bgaA*::*kan*1t2-P_{fcsK}-*pcsB*$^+$ (amplicon from IU1979 × IU2592)	Erm^r Kan^r	This study
IU2824	D39 Δ*dacA*::P_c-*aad9* (amplicon from IU1705 × IU1690)	Spec^r	This study
IU2825	D39 Δ*cps*2A′ (*cps*2BCDETFG)H′ Δ*dacA*::P_c-*aad9* (amplicon from IU1705 × IU1945)	Spec^r	This study
IU3192	D39 Δ*cps2BCDE*<>*kan-rpsL* (amplicon from IU1783 × IU1690)	Kan^r	This study

[a] Strains are derivatives of *S. pneumoniae* EL59 (R6) and IU1690 (D39), unless indicated otherwise. Strains were constructed by transformation (indicated by ×) of indicated recipients with PCR fragments amplified from the chromosomes of other strains or synthesized by fusion PCR (see Materials and Methods). <> or :: indicates exact replacement of a reading frame or insertion, respectively.

[b] Antibiotic resistance markers: Spec^r, spectinomycin; Erm^r, erythromycin; Kan^r, kanamycin; Str^r, streptomycin; Amp^r, ampicillin (in *E. coli* strains only).

[c] IU1945 was constructed to have the same Δ*cps* region as EL59 (R6) (33).

Tris-HCl, pH 7.4, 150 mM NaCl, 2 mM KCl), and glycerol and BSA were added to final concentrations of 20% (vol/vol) and 5% (wt/vol), respectively. Purified antibody was dispensed into 100-μl volumes and stored at −20°C.

Purification of His_6-(N)-MreC and production of antibody. His_6-(N)-MreC lacking the 32-amino-acid transmembrane domain from its amino terminus was overexpressed in *E. coli* BL21(DE3) cells (Invitrogen) from plasmid pET15b::*mreC′*, which was constructed by conventional methods using the primers listed in Table S1 of the supplemental material that contained added NdeI and XhoI restriction sites. A 200-ml culture was grown in LB broth containing 100 μg ampicillin per ml at 30°C to an OD_{620} of ≈0.4 and induced by the addition of 1 mM IPTG for 3 h. Cells were collected and disrupted as described above. All of the His_6-(N)-MreC was recovered as inclusion bodies in the pellet, which were solubilized in 50 mM $NaPO_4$, pH 7.0, 6 M guanidine-HCl, 300 mM NaCl. Further purification was performed with a Talon metal affinity resin

(Clontech Laboratories) using the manufacturer's instructions for purification of insoluble polyhistidine-tagged proteins. The protein was eluted from the Talon resin with 45 mM $NaPO_4$, pH 7.0, 270 mM NaCl, 150 imidazole, 5.4 M guanidine-HCl in a 2-ml gravity column. The eluate (1 ml) was dialyzed overnight at 25°C in 50 mM $NaPO_4$, pH 7.0, 300 mM NaCl, 8 M urea (storage buffer) and run on an SDS-PAGE gel. Purity was estimated at >99% by Coomassie staining, and protein recovery was 1.3 mg, as determined by the RC/DC protein assay (Bio-Rad). Rabbit polyclonal antibody against purified His_6-(N)-MreC protein was prepared by Cocalico Biologicals. The anti-MreC antibody preparation was not purified further, because it bound to only one band at 29.7 kDa corresponding to MreC in Western blot assays of pneumococcal cellular extracts and did not react with extracts prepared from an R6 Δ*mreCD* mutant (data not shown).

Preparation of secreted and cell-associated proteins. Cultures were grown exponentially as described above to an OD_{620} of ≈0.2, and 1-ml samples were microcentrifuged (21,000 × *g*; 10 min; 25°C). Pellets of cells (≈90% yield) were lysed directly by resuspension in 100 μl of lysis buffer (1% ([vol/vol] SDS, 0.1% [vol/vol] Triton X-100). Protein concentrations were determined by the DC protein assay with BSA as the standard (Bio-Rad). An 80-μl aliquot of lysed pellet was mixed with 80 μl of 2× SDS-PAGE sample buffer (58) containing freshly added 5% (vol/vol) 2-mecaptoethanol, and cell-associated proteins were analyzed by SDS-PAGE (see below). Supernatants were filtered through an Acrodisc 0.22-μm Supor membrane filter (Pall Sciences), and proteins in the supernatants, including those from the medium, were precipitated by the addition of 100% (wt/vol) trichloroacetic acid to a final concentration of 20% (wt/vol) on ice. After 15 min, precipitated proteins were collected by microcentrifugation (21,000 × *g*; 5 min; 4°C), washed once with 800 μl of ice-cold 100% ethanol, and allowed to air dry at room temperature. Trichloroacetic acid-precipitated secreted proteins were resuspended in 80 μl of 2× SDS sample buffer containing freshly added 5% (vol/vol) 2-mercaptoethanol and subjected to SDS-PAGE.

SDS-PAGE and immunoblot analyses. All SDS samples were boiled for 5 min before loading onto 4% stacking, 10% separating SDS-PAGE gels containing Tris-glycine buffer (58). Usually 15 μg of cell-associated protein from pellet extracts was loaded per lane, and a corresponding volume of secreted protein sample was loaded into a separate lane on the same gel. After electrophoresis, proteins were electrophoretically transferred to nitrocellulose membranes in Towbin buffer (above). Immunodetection was carried out by blocking membranes with 5% ECL reagent (Amersham) in PBS-T (0.1% [vol/vol] Tween 20 in 1× PBS, pH 7.4) for 20 min at 25°C according to the manufacturer's instructions. Affinity-purified anti-PcsB antibody (1:500), anti-FLAG antibody (anti-M2 polyclonal; 1:1,000; Sigma), or unpurified anti-MreC serum (1:1,000) was diluted by the factors in the PBS-T, and membranes were incubated for 1 h at 25°C with gentle shaking. Horseradish peroxidase-conjugated anti-rabbit secondary antibody (Amersham) was diluted 1:10,000 in PBS-T, and incubation was continued 1 h at 25°C with shaking. ECL detection reagents (Amersham) in a 1:1 ratio were added to the membrane directly prior to autoradiography or quantitation. Autoradiography was done using 1- or 5-min exposures on Biomax XAR scientific imaging film (Kodak). Blots were directly quantitated using an IVIS Xenogen VivoVision Lumina system and software (1- to 3-min exposure, F-stop 2, stage setting B, high-resolution/small binning). Absolute and relative amounts of cell-associated and secreted PcsB were normalized back to equivalent amounts in 1 ml of culture (≈1×10^8 to 2×10^8 CFU).

Microscopy. Samples of 100 μl of cultures growing exponentially in BHI broth were taken at an OD_{620} of ≈0.2 to 0.3 and stained without fixation by adding 4′,6-diamidino-2-phenylindole (DAPI) and a 1:1 mixture of vancomycin and Bodipy-FL-conjugated vancomycin (FL-Van; Molecular Probes) to final concentrations of 0.2 μg per ml and 2.0 μg per ml, respectively, for 10 min in the dark at room temperature (41). A 0.7-μl aliquot of stained bacteria was placed on a clean glass slide to which a coverslip was added. Cells were examined using a Nikon E-400 epifluorescence phase-contrast microscope equipped with a mercury lamp, a 100× Nikon Plan Apo oil-immersion objective (numerical aperture, 1.40), and filter blocks for fluorescence (DAPI, EX 330 to 380, DM 400, and BA 435 to 485; FL-Van, EX 460 to 500, DM 505, and BA 510 to 560). Images were captured using a cooled digital SPOT RT monochrome camera and processed with SPOT Advanced software. Length-to-width aspect ratios (ARs) were determined from phase-contrast micrographs by using Nikon NIS-Elements AR software. A total of 25 to 50 individual cells from three separate cultures were measured for each strain. Cells with sufficiently demarcated boundaries to allow measurements were chosen as randomly as possible. Two-tailed *t* tests were performed on average ARs by using GraphPad Prism software.

Preparation of lactoyl-peptides. Methods reported in reference 2 were modified as follows. Exponentially growing 200-ml cultures (OD_{620}, ≈0.2 to 0.3) were harvested by centrifugation (14,300 × *g*; 20 min; 4°C). Pellets were resuspended in 15 ml of PBS and added to 10 ml of boiling 10% SDS in an Oakridge tube. The mixture was then boiled for 30 min more. SDS-insoluble material containing PG was collected by centrifugation (30,000 × *g*; 20 min; 20°C). Pellets were washed by resuspension three times with 25 ml H_2O followed by centrifugation (30,000 × *g*; 15 min; 20°C). Pellets were resuspended in 3 ml of H_2O and transferred to two 1.5-ml microcentrifuge tubes, and insoluble material was collected by microcentrifugation (21,000 × *g*; 5 min; 25°C). Pellets were combined in 1 ml of 50 mM $NaPO_4$ (pH 7.4) and 200 μg trypsin (Sigma) per ml. Following overnight (≈16 h) incubation at 37°C with shaking (400 rpm), pellets were collected by microcentrifugation (21,000 × *g*; 5 min; 25°C). Pellets were washed with complete suspension followed by centrifugation in the following series of buffers: three times in 1 ml of 1% (vol/vol) SDS, once in 1 ml of 8 M LiCl (with 15-min incubation at 37°C and shaking at 400 rpm), once in 1 ml of 0.1 M EDTA (with 15-min incubation at 37°C and shaking at 400 rpm), and three times in 1 ml of H_2O. Pellets were resuspended in a final volume of 400 μl containing 25 mM $NaPO_4$, pH 6.0, 0.5 mM $MgCl_2$, 40 μg mutanolysin (Sigma) per ml, and 200 μg lysozyme (Sigma) per ml and incubated at 37°C overnight (≈16 h) with shaking at 400 rpm. Mixtures were heated at 95°C for 3 min and insoluble material removed by ultracentrifugation (104,000 × *g*; 30 min; 25°C). Supernatants were divided in half (200 μl each), and 64 μl of ammonium hydroxide (stock of 29%) was added to each 200-μl sample, which was incubated at 37°C for exactly 5 h. Each sample was neutralized by the addition of 61 μl of concentrated glacial acetic acid. The resulting lactoyl-peptide samples were briefly frozen on dry ice, lyophilized overnight (≈16 h), and then stored at −20°C. Samples were dissolved in 200 μl of 0.05% (vol/vol) trifluoroacetic acid (TFA; stock at 100%). Insoluble material was removed by microcentrifugation (21,000 × *g*; 15 min; 25°C). Supernatants were transferred to new microcentrifuge tubes and entire 200-μl samples were subjected to reverse-phase high-performance liquid chromatography (RP-HPLC).

RP-HPLC analysis of lactoyl-peptides and method validation. Lactoyl-peptides were resolved by RP-HPLC using a C_{18} column (Vydac 218 TP54; 4.6 by 250 mm) at a flow rate of 0.5 ml per min at 30°C attached to a Shimadzu 10A HPLC system. The mobile phases were solvent A (0.05% [vol/vol] TFA in water) and solvent B (0.035% [vol/vol] TFA in acetonitrile). Lactoyl-peptides were eluted with the following gradient: 100% solvent A from 0 to 10 min; 0 to 20% solvent B from 10 to 100 min; and 20% solvent B from 100 to 120 min. Eluted lactoyl-peptides were detected by UV absorption at 210 nm. Fractions were collected and subjected to mass spectrometry (MS) analysis as described below. Integration of areas of individual peaks was performed using Class-VP software (Shimadzu). Baselines were set "valley to valley" because of reproducible baseline changes during the course of the runs (see the supplemental material).

This method to analyze PG peptide composition was previously validated and used for several gram-positive bacteria, including *Enterococcus* and *Lactobacillus* species (2, 6, 7). We validated this method for pneumococcus in the following ways. (i) Total yields of lactoyl-peptides from strains grown to similar densities (OD_{620}, ≈0.2 to 0.3) were compared by summing all areas from chromatograms. The yields of lactoyl-peptides in arbitrary mvolt area units, and by inference PG content, were similar for the unencapsulated strains R6 ($4.0 \times 10^7 \pm 0.6 \times 10^7$) and D39 Δ*cps* ($4.5 \times 10^7 \pm 1.1 \times 10^7$) and encapsulated strain D39 ($3.4 \times 10^7 \pm 0.7 \times 10^7$) (data not shown). We noted that PG preparations from encapsulated strains formed less-compact pellets, which could be partially lost during the multiple rounds of centrifugation in the purification procedure, compared to those of unencapsulated strains. PG preparations from strain D39 in which material was obviously lost were not included in the above calculation of yield, and the relative amounts of lactoyl-peptides within chromatograms were independent of the amount of PG recovered for analysis (data not shown). (ii) We did not obtain statistically different total yields of lactoyl-peptides (or PG) from unencapsulated or encapsulated strains underexpressing PcsB compared to their *pcsB*$^+$ parent strains (data not shown). (iii) The release of lactoyl-peptides from purified PG was quantitative for unencapsulated and encapsulated strains. To determine the efficiency of release from purified PG, we added 5 μCi of [^{14}C]lysine (11.2 GBq/mmol, 1.85 MBq per ml; Amersham Biosciences) or 0.25 μCi [^{3}H]choline (3.03 TBq/mmol, 37 MBq per ml; Amersham Biosciences) to 200 ml of BHI broth, which was inoculated with unencapsulated R6 or encapsulated D39 as described above. PG was purified and digested with mutanolysin and lysozyme as described above. We found 85 to 95% of the ^{14}C-labeled PG peptides and ^{3}H-labeled PG teichoic acid was released as soluble material from the insoluble PG, independent of capsule. This efficiency of release of PG peptides is comparable to that reported previously for other gram-positive bacteria using this procedure (2, 6, 7). (iv) Consistent with labeling experiments, we obtained similar recoveries of lactoyl-peptides and chromatograms from encapsulated D39 and an isogenic unencapsulated D39 Δ*cps* mutant (see Results), indicating that capsule did not affect muropeptide release in this method. (v) We obtained similar chromatograms and relative yields of PG peptides by this

method for the R6 and D39 strains as those determined previously by a different method that used amidase digestion to release pneumococcal cell wall stem peptides (see Table S2 in the supplemental material) (25, 60, 61).

MS analysis of lactoyl-peptides. Fractions from RP-HPLC were infused directly through a custom-built nanospray source into an LCQ Deca XP ion trap mass spectrometer (ThermoElectron, Waltham, MA) at 500 nl per min. Mass spectra from 250 to 2,000 Da were averaged for 1 min for each sample. Lactoyl-peptide ions were further analyzed by tandem MS over the mass range from about one-quarter of the precursor *m/z* to two times the precursor *m/z* or 2,000 Da, again with signal averaging for 1 min. Structural assignments for the tandem mass spectra are reported in the supplemental material and were made by adding a lactoyl group to the chemical structures of stem peptides previously reported for pneumococcus (26, 61, 63).

Penicillin sensitivity assays. Ten-ml cultures growing exponentially to an OD_{620} of ≈0.1 to 0.2 in BHI broth were split into two 16-mm-diameter tubes, to which penicillin G (Sigma) was added to a final concentration of 0.01 or 0.1 μg per ml (≈10× the MIC). Density was monitored at OD_{620} every 30 min for 3 to 5 h, and data were plotted using GraphPad Prism software.

RNA extraction and QPCR analyses. Total pneumococcal RNA was prepared by a rapid lysis procedure and analyzed by quantitative PCR (QPCR) as described before (53). Two sets of PCR primers covering the central (PCR1) or 3′ region (PCR2) of the pcsB transcript (see Table S1 in the supplemental material) were used for RNA quantitation. Both sets of primers showed standard curves with R^2 values of >0.985 and 90 to 110% reaction efficiencies and only one peak in dissociation curves. *pcsB*$^+$ transcript amounts were normalized to 16S rRNA amounts as described previously using primers in Table S1 of the supplemental material (53).

Microarray analyses. Microarray analyses were performed comparing relative transcript amounts of strains IU1533 with those of IU1979 (Table 1) grown exponentially in BHI broth (see Fig. S2 in the supplemental material). Total RNA was prepared at an OD_{620} of 0.2 as described above. *S. pneumoniae* microarrays were purchased from Ocimum Biosolutions. Synthesis, labeling, hybridization, scanning, normalization, and analysis using the Cyber-T web interface were performed as described previously (53).

Microarray data accession number. Intensity and expression ratio data for all transcripts have been deposited in the GEO database, accession number GSE13107.

RESULTS

PcsB is essential in serotype 2 *S. pneumoniae*. We reported previously that we were unable to knock out the *pcsB*$^+$ gene in laboratory strain R6 (45), which is an unencapsulated mutant originally isolated from a derivative of virulent serotype 2 strain D39 (33). However, a recent report claims that *pcsB* can be knocked out in serotype 4 (TIGR4) and 6B (PJ-1259) clinical isolates, although the growth of the Δ*pcsB* mutants appeared to be severely impaired (29). Consequently, we reprised experiments to test the essentiality of *pcsB*$^+$ in serotype 2 strains. We attempted to perform *pcsB* knockout experiments in the parent R6 and D39 strains and in mutants containing ectopic copies of *pcsB*$^+$ inserted into *bgaA* (Fig. 1B), which encodes an extracellular β-galactosidase that degrades human glycoproteins (9). In these ectopic constructs, *pcsB* transcription was driven by a synthetic constitutive promoter (P_c) (37) or by a fucose-inducible promoter (P_{fcsK}) (10). The knockout mutations tested were a Δ*pcsB*<>P_c-*ermAM* or a Δ*pcsB*<>*ermAM* deletion/replacement in which the entire *pcsB*$^+$ reading frame was replaced by a P_c-*ermAM* cassette (from strain IU1547) (Table 1) (45) or by the *ermAM* reading frame alone (from strain IU1979) (Table 1), respectively (Fig. 1A).

In numerous independent transformations, we were unable to cross amplicons containing the Δ*pcsB*<>P_c-*ermAM* or Δ*pcsB*<>*ermAM* knockout mutation into the native *pcsB* locus of R6 or D39 when transformation plates were incubated for 3 days at 37°C in an atmosphere of 5% CO_2. In contrast, the Δ*pcsB*<>P_c-*ermAM* or Δ*pcsB*<>*ermAM* mutation readily crossed into R6 or D39 strains expressing PcsB from the ectopic Δ*bgaA*′::P_c-*pcsB*$^+$ site, and transformants appeared overnight (Fig. 1B and data not shown). Consistent with these results, Δ*pcsB*<>*ermAM* Δ*bgaA*′::P_{fcsK}-*pcsB*$^+$ mutants in R6 (IU2801) and D39 (IU2539) (Table 1) were constructed by transformations on TSAII BA plates containing 0.2% (wt/vol) fucose. IU2801 and IU2539 grew like their parent strains in BHI broth containing 0.8% to 1.2% (wt/vol) fucose but abruptly ceased growth following resuspension in BHI broth lacking fucose (data not shown). Likewise, R6 and D39 mutants IU1545 and IU2091 (Table 1), in which the intercistronic region between *pcsB* and upstream *mreD* was replaced by a *kan* marker, transcription terminators, and a P_{fcsK} promoter driving *pcsB*$^+$ (Fig. 1C), grew normally in BHI broth containing fucose but ceased growing when fucose was removed. (data not shown) (45). Removal of fucose led to severe depletion of PcsB in these mutants and formation of greatly distorted cells (see below) (45). PcsB-depleted cultures did not resume growth during overnight incubation and usually did not lyse (data not shown). Together, these results support the conclusion that *pcsB* is essential in serotype 2 strains of *S. pneumoniae.*

PcsB exists as a single processed species. To correlate PcsB expression with phenotypes, we determined the relative amounts of PcsB in parent strains and the mutants shown in Fig. 1 by quantitative Western blotting (see Materials and Methods). As reported previously for PcsB orthologs from *S. mutans* and *S. agalactiae* (11, 40, 56), a significant amount of PcsB was secreted directly into the medium during exponential growth of these serotype 2-derived strains in BHI broth (fraction secreted, 77 ± 5% for D39 [Fig. 2A]; 62 ± 4% for D39 Δ*cps* [IU1945]; 47 ± 6% for R6 [data not shown]). In contrast to a previous report (42), we observed only a single band of the same molecular mass (41.9 kDa) for the secreted and cell-associated PcsB, suggesting that all PcsB is processed during secretion by the Sec system. Similar results were obtained for unencapsulated strains R6 and IU1945 (D39 Δ*cps*) (data not shown). We confirmed this conclusion in two ways. We attached a FLAG epitope tag of 8 amino acids to the C terminus of PcsB expressed from the native locus in R6 and D39. These mutants (IU1845 and IU2105 [Table 1]) were constructed by cotransformation with a P_c-*ermAM* cassette in the downstream intercistronic space between *pcsB* and *rpsB* (Fig. 1A) (45). The resulting strains did not display defects in cell morphology (data not shown). Again, we detected only a single band of the same M_r for the cell-associated and secreted forms of PcsB-(C)-FLAG, which had a slightly greater M_r (42.8) than native PcsB (Fig. 2A). Last, we constructed a R6 *pcsB*$^+$ Δ*bgaA*′::P_{fcsK}-*pcsB* (A27D) merodiploid containing a defective signal peptide cleavage site in PcsB (IU2718 [Table 1]). This strain grew poorly in CDM containing fucose and produced both processed (PcsB, 41.9 kDa) and unprocessed (SP-PcsB, 45.0 kDa) cell-associated PcsB, in contrast to the R6 parent, which only produced processed PcsB (Fig. 2B). The SP-PcsB band was not produced in the absence of fucose (data not shown). Thus, unprocessed SP-PcsB was clearly resolved in this PAGE system, further supporting the claim that all PcsB is normally processed in bacteria growing under these conditions.

Relative PcsB and MreC expression levels in *pcsB* mutants. To interpret results of phenotype tests, we determined the

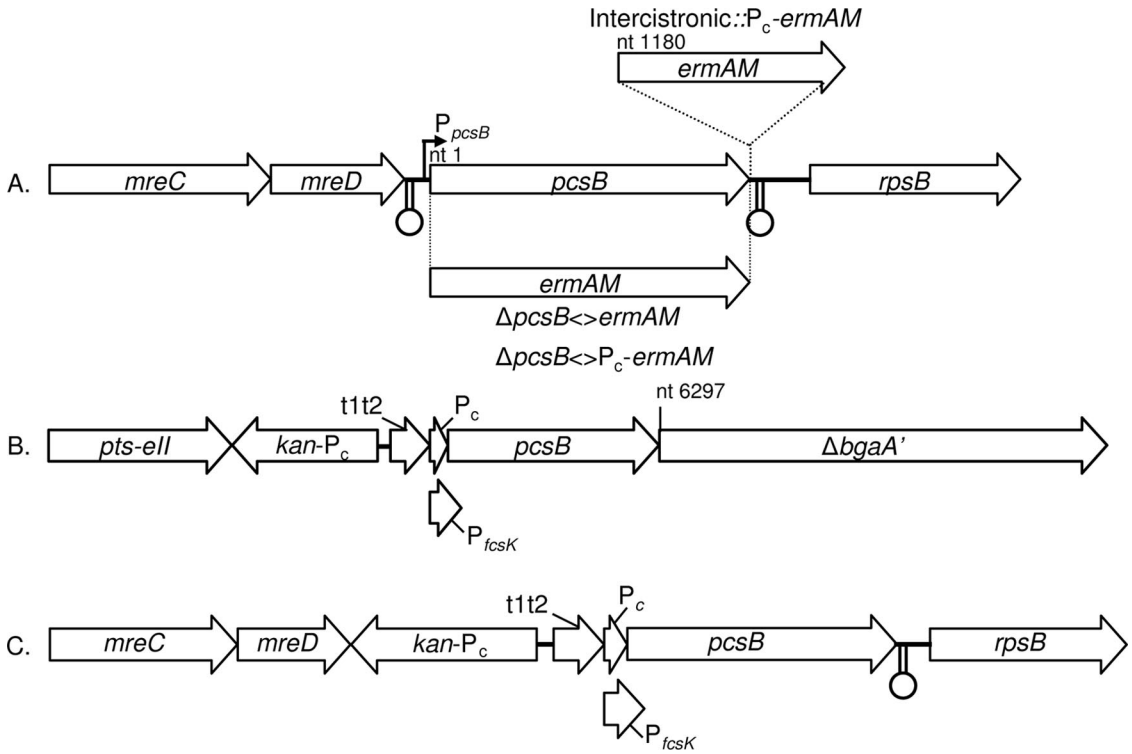

FIG. 1. Genetic constructs used in this study (drawn to scale). See Table 1 for strains. (A) The native *pcsB* locus showing the upstream *mreCD* genes and the downstream *rpsB* gene that encodes a ribosomal protein. The Δ*pcsB*<>*ermAM* and Δ*pcsB*<>P$_c$-*ermAM* reading frame replacements of *pcsB* are indicated along with the mapped internal P$_{pcsB}$ promoter (L.-T. Sham, unpublished result) and putative terminators (lollipops). The location of the intercistronic P$_c$-*ermAM* insertion used as a marker in some constructs is indicated 1,180 nucleotides downstream from the *pcsB* start codon. (B) Structures of the Δ*bgaA'*:: *kan*t1t2-P$_c$-*pcsB*$^+$ and Δ*bgaA'*:: *kan*t1t2-P$_{fcsK}$-*pcsB*$^+$ constructs used for ectopic expression of PcsB in strains IU1979, IU2801, and IU2537. The *kan*t1t2-P$_c$-*pcsB*$^+$ or *kan*t1t2-P$_{fcsK}$-*pcsB*$^+$ constructs contain the constitutive synthetic P$_c$ promoter and *ermAM* ribosome binding site (37) or the fucose-inducible P$_{fcsK}$ promoter and *fcsK* ribosome binding site (10), respectively, and the t1t2 ribosome operon terminators from *E. coli* to block transcription from upstream of P$_c$ and P$_{fcsK}$ (46). The constructs were inserted between the end of *pts-eII* and a deletion of the promoter-proximal region of *bgaA* that extended 6297 nucleotides from the translation start codon of *bgaA*. (C) Insertion of the *kan*t1t2-P$_c$-*pcsB*$^+$ and *kan*t1t2-P$_{fcsK}$-*pcsB*$^+$ constructs into the native *pcsB* locus. The constructs replaced the intercistronic region between *mreCD* and *pcsB*, which included the putative terminator and P$_{pcsB}$ internal promoter shown in panel A. No known transcription terminator follows the divergently transcribed *kan* gene in these constructs.

relative amounts of PcsB in this set of mutant constructs. A R6 Δ*pcsB*<>*ermAM* Δ*bgaA'*::P$_c$-*pcsB*$^+$ mutant (IU1979 [Table 1]) (Fig. 1A and B) produced ≈7-fold less PcsB than its R6 *pcsB*$^+$ parent (Table 2), and the relative expression of PcsB was even less in the corresponding D39 mutant (IU2537 [Table 1]) (Table 2). Reverse transcription-PCR of R6 and D39 showed that *pcsB* is cotranscribed to some extent with the upstream *mreCD* genes (Fig. 1), which encode homologs of the MreCD cell shape proteins in rod-shaped bacteria (5, 20, 36; A. D. Land, unpublished result). Therefore, we also tested whether the MreC amount changed in these *pcsB* mutants. The Δ*pcsB*<>*ermAM* deletion/replacement mutation in strains IU1979 and IU2801 caused a slight (<1.5-fold) decrease in the relative amount of MreC compared to their R6 parents (Table 2). Consistent with this result, no decrease in relative *mreCD* transcript amount was detected in strain IU1979 in microarray analyses using a cutoff of 1.8-fold (below). There was again a small strain difference between D39 and R6 in that the relative MreC amount dropped ≈1.8-fold in the corresponding D39 Δ*pcsB*<>*ermAM* mutant (Table 1; Table 2). Control strain IU2547 (Table 1) containing a Δ*bgaA'*::P$_c$-*aad9* deletion/insertion produced MreC amounts comparable to that of the D39 parent (Table 2).

P$_c$-*pcsB*$^+$ constructs at the native *pcsB* locus of R6 and D39 (IU1744 and IU1807) (Table 1; Fig. 1C) produced ≈4-fold less PcsB and ≈2-fold less MreC than their parent strains (Table 2). P$_c$-*pcsB*$^+$ constructs in the native *pcsB* locus consistently produced more PcsB than those in the ectopic *bgaA* site (Table 2), possibly because of transcript instability caused by fusion into the *bgaA* site (Fig. 1B and unpublished results). The greater expression of PcsB from the P$_c$-*pcsB*$^+$ constructs in the native *pcsB* locus than in the *bgaA* locus was reflected by shorter lags and higher relative growth rates and yields of the corresponding strains (see Fig. S1 and S2 in the supplemental material). IU1744 containing a recombinant plasmid that expressed *pcsB* under the control of the inducible P$_{mal}$ promoter (IU2564 [Table 1]) increased the PcsB amount ≈2.6-fold and ≈10-fold compared to R6 and the vector control strain (IU2608), respectively (Table 2). The relative MreC amounts in strains IU1744, IU2608, and IU2564, which contained a P$_c$-*kan* cassette oppositely transcribed into *mreCD* (Fig. 1B), were comparably decreased by ≈2-fold (Table 2).

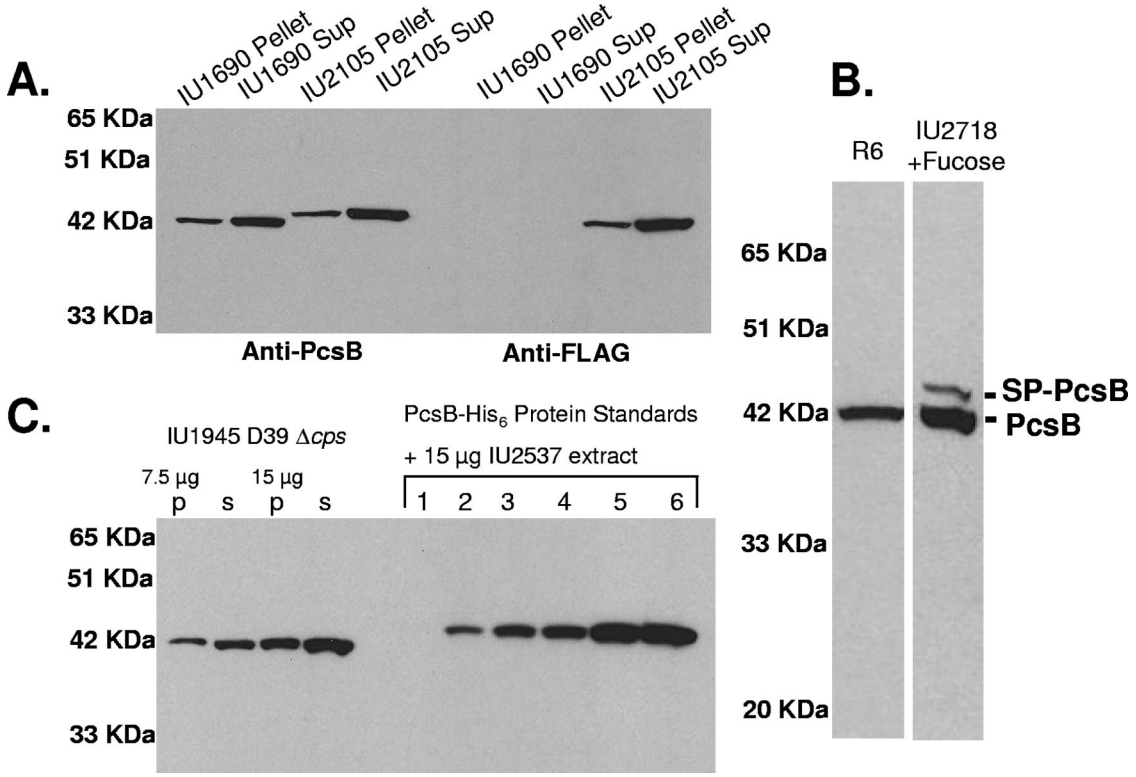

FIG. 2. Western immunoblot analyses of cell-associated (pellet) and secreted (supernatant) PcsB. (A) Demonstration that all cell-associated and secreted PcsB is processed to the same M_r. IU1690 (D39 parent) and IU2105 expressed wild-type (41.9 kDa) and C-terminal FLAG-tagged PcsB (42.8 kDa), respectively. The left four lanes or right four lanes were probed with affinity-purified anti-PcsB or commercial anti-FLAG antibody, respectively, as described in Materials and Methods. The autoradiogram is representative of several independent experiments but was not used for quantitation, because the signal was not strictly linear with concentration. Instead, blots were quantitated directly by using an IVIS imaging system (see Materials and Methods). (B) Production of cell-associated unprocessed (SP-PcsB; M_r, 45.0) and processed (PcsB; M_r, 41.9) PcsB by R6 *pcsB*$^+$ Δ*bgaA′*::P$_{fcsK}$-*pcsB* (A27D) merodiploid strain IU2718 grown in CDM containing 0.8% (wt/vol) fucose. A 28-μg aliquot of pellet extract from IU2718 was loaded and Western blots were probed with purified anti-PcsB antibody (see above). A pellet extract from R6 grown in CDM was included as a marker on the same gel. Intervening lanes were removed from the figure. (C) Quantitation of the absolute amount of cell-associated PcsB was performed as described in Materials and Methods using affinity-purified anti-PcsB antibody. A representative autoradiogram is shown of the PcsB produced from 7.5 and 15 μg (used in quantitation) of extract prepared from cell pellets (p) of D39 Δ*cps* strain IU1945 and the corresponding amount of secreted (s) PcsB recovered from the medium (see Materials and Methods). Purified PcsB was spiked into extracts of strain IU2537, which greatly underexpressed PcsB (Table 2), at the following amounts in lanes 1 to 6: 0.001 μg, 0.005 μg. 0.008 μg, 0.010 μg, 0.050 μg, and 0.10 μg, respectively. Quantitation was performed directly from blots by using an IVIS imaging system and not from autoradiograms, such as the one shown. See text for additional details.

Finally, P$_{fcsK}$-*pcsB*$^+$ constructs at the native *pcsB* locus in R6 and D39 (IU1545 and IU2091) (Table 1; Fig. 1C) or inserted into *bgaA* (Fig. 1B) in a Δ*pcsB*<>*ermAM* mutant of R6 (IU2801) produced about the same amount of PcsB as the parent strains when grown exponentially in BHI broth containing 0.2% to 1.2% (wt/vol) fucose (Table 2). Five hours after a shift to medium lacking fucose (see Materials and Methods), very little PcsB was detected in IU1545 or IU2091, and quantitation was difficult (Table 2). The amounts of MreC were comparable in strains IU1545 and IU2091 before or after fucose deprivation (Table 2). Together, these data show that this set of mutants exhibited a range of PcsB expression, and insertion mutations in the native *pcsB* locus generally caused a slight decrease in MreC amount; however, there was no significant change in MreC amount when PcsB was overexpressed or severely depleted.

Cell-associated PcsB is relatively abundant in *S. pneumoniae*. We determined the cellular amounts of PcsB in the D39 Δ*cps* and R6 strains growing exponentially in static BHI broth at 37°C in an atmosphere of 5% CO_2 (see Materials and Methods). For this quantitation, we loaded 15 μg of protein from pellet extracts in each lane of the PAGE gel (Fig. 2C). For standards, we used PcsB-(C)-His$_6$ purified from *E. coli* (see Materials and Methods). To prevent artifacts caused by higher transfer efficiencies of purified proteins (22), we prepared a standard series by spiking known concentrations of purified PcsB-(C)-His$_6$ into 15 μg of crude extract of strain IU2537 (Δ*pcsB*<>*ermAM* Δ*bgaA′*::P$_c$-*pcsB*$^+$) which produced very low amounts of PcsB (Table 2). The amounts of PcsB detected in D39 Δ*cps* and R6 extracts and in the standard series were linear with amount, and the amounts of PcsB in the D39 Δ*cps* and R6 extracts fell within standard curves (data not shown). We detected 0.15 ± 0.08 μg of cell-associated PcsB per 223 ± 20 μg of D39 Δ*cps* extract (Fig. 2C), which corresponded to ≈2 × 10^8 CFU, with the vast majority of cells diplococci (see below). Since the M_r of processed PcsB is 41.9,

TABLE 2. Relative amounts of PcsB and MreC in mutants used in the study[a]

Strain	Relevant genotype	Relative PcsB amt (%)	Relative MreC amt (%)
EL59[b]	R6 parent	≡100 (4,400 ± 1,400 monomers bound/cell)	≡100
IU1979	R6 Δ*pcsB*<>*ermAM* Δ*bgaA*′::P_c-*pcsB*$^+$	14 ± 6	68 ± 21
IU2801[c]	R6 Δ*pcsB*<>*ermAM* Δ*bgaA*′::P_{fcsK} -*pcsB*$^+$	+fucose: 110 ± 26	91 ± 9
IU1744	R6 P_c-*pcsB*$^+$ (native locus)	21 ± 5	38 ± 9
IU2608[c]	R6 IU1744 (pLS1RGFP; vector)	+maltose: 24 ± 5	+maltose: 43 ± 2
IU2564[c]	R6 IU1744 (pLS1RGFP::P_{mal}-*pcsB*$^+$)	+maltose: 256 ± 105	+maltose: 62 ± 11
IU1545[c,e]	R6 P_{fcsK}-*pcsB*$^+$ (native locus)	+fucose: 84 ± 28; −fucose: < 8	+fucose: 22 ± 1; −fucose: 21 ± 7
IU1983[d]	R6 Δ*mreCD*::*aad9*	98 ± 5	None detected
IU1690[b]	D39 parent	≡100	≡100
IU2537[e]	D39 Δ*pcsB*<>*ermAM* Δ*bgaA*′::P_c-*pcsB*$^+$	<3	55 ± 8
IU2547	D39 Δ*bgaA*′::*aad9* (control)	76 ± 15	95 ± 11
IU1807	D39 P_c-*pcsB*$^+$ (native locus)	29 ± 14	53 ± 17
IU2091[c,e]	D39 P_{fcsK}-*pcsB*$^+$ (native locus)	+fucose: 140 ± 35; −fucose: <3	+fucose: 25 ± 3; −fucose: 40 ± 13
IU2102[d]	D39 Δ*mreCD*<>*aad9*	85 ± 5	None detected
IU1945[b]	D39 Δ*cps*	≡100 (5,400 ± 3000 monomers bound/cell)	≡100
IU2336	D39 Δ*cps* P_c-*pcsB*$^+$ (native locus)	13 ± 3	49 ± 20

[a] Relative PcsB and MreC amounts were determined by quantitative Western blotting normalized to total protein amounts (see Fig. 2 and Materials and Methods). Amounts are relative to R6, D39, and D39 Δ*cps* parent strains run on the same immunoblots. Cell-associated and secreted PcsB were added to give total amounts, and the fraction of secreted PcsB (see Results) did not change in R6 and D39 strains underexpressing PcsB (data not shown). All amounts represent at least three biological replicates, except for IU2608, IU2564, and IU2102, which were done twice. Standard errors of the means are indicated.

[b] The average number of cells per chain used in calculations was 3 or 2 for EL59 or IU1945, respectively, based on counting fields of several hundred cells by phase microscopy. The amounts of PcsB and MreC in IU1690 were comparable to those in strains EL59 and IU1945 when run on the same Western blots (data not shown). We quantitated PcsB amount per cell in IU1945 instead of IU1690, because IU1945 was predominantly diplococcal whereas IU1690 formed chains of various lengths (Fig. 5 and data not shown).

[c] 1.2 % (wt/vol) fucose (IU2801), 0.2% (wt/vol) fucose (IU1545 and IU2091), or 1% (wt/vol) maltose (IU2608 and IU2564) was added to cultures. Shifts to medium lacking fucose to deplete PcsB amounts were performed as described in Materials and Methods.

[d] No MreC was detected in autoradiograms or by an IVIS imaging system (see Materials and Methods).

[e] The amounts of PcsB in IU1545, IU2537, and IU2091 (−fucose) were below the limit of reliable quantitation, although very faint bands could be detected on autoradiograms exposed for long periods of time.

then ≈5,400 monomers of PcsB were bound per cell (Table 2). We detected comparable amounts of cell-associated PcsB in R6 (≈4,400 monomers per cell based on 0.09 ± 0.03 μg of cell-associated PcsB per 243 ± 4 μg per ≈1×10^8 CFU), which mainly formed diplococci or short chains of four under these growth conditions (Table 2). Thus, PcsB is a moderately abundant protein in *S. pneumoniae.*

Capsule influences cell shape and chain formation in wild-type D39 and during PcsB underexpression. There was a strong correlation between the amount of PcsB expressed (Table 2) and defects in cell morphology (Fig. 3 and 4). As we reported previously, the R6 parent strain formed mainly ovoid cells (AR, 1.62) in short chains of two or four cells (Fig. 5, bar 1). R6 cells were stained by FL-Van at their equators, septa, or sometimes both (Fig. 3), indicating likely regions of PG biosynthesis (13, 45, 51). Moderate underexpression of PcsB in strain IU1744 (P_c-*pcsB*$^+$ [native locus]) and IU1979 (Δ*pcsB*<>*ermAM* Δ*bgaA*′::P_c-*pcsB*$^+$) (Table 2) resulted in the formation of longer chains of uniformly shaped cells (Fig. 3B and C and 5, bars 2 and 3). These cells were substantially more spherical (AR, 1.09 and 1.15), but with comparable widths to R6 (Fig. 5, bars 1 to 3), and they stained with FL-Van at nearly every junction between cells compared to R6 (Fig. 3A to C). Complementation of strain IU1744 with a plasmid that overexpressed PcsB by about 2.6-fold (IU2564; Table 2) reversed all shape and chain formation defects (Fig. 3E) and confirmed that these phenotypes were caused by PcsB underexpression. This conclusion was further supported by the observation that Δ*mreCD* mutants could readily be constructed in R6 and D39 and did not show any defects in cell growth or division (data not shown) (see Discussion). These Δ*mreCD* mutants totally lacked MreC, as expected, and contained wild-type levels of PcsB (Table 2). Thus, the small drop in MreC expression observed in strain IU1744 and other *pcsB* mutants (Table 2) was not the cause of these cell division phenotypes (Fig. 3).

Unexpectedly, moderate underexpression of PcsB in encapsulated strain D39 caused different shape and chain formation phenotypes than those in the R6 background. Parent strain D39 grown exponentially in BHI broth formed medium-length chains of 11 ± 1 mostly uniform, ovoid cells (Fig. 4A and 5, bar 4). PcsB was underexpressed in D39 mutant IU1807 (P_c-*pcsB*$^+$ [native locus]) to about the same level as in the R6 IU1744 mutant described above (Fig. 3B; Table 2). This moderate underexpression of PcsB in D39 resulted in three new phenotypes. In contrast to IU1744 compared to R6, IU1807 formed more short chains of cells than IU1690 (Fig. 5, bars 4 and 5). Most of the IU1807 cells were only slightly less ovoid (AR, 1.47) than IU1690 cells (AR, 1.69), but not nearly as spherical as IU1744 cells (AR, 1.09) (Fig. 5, bars 2, 4, and 5), where these AR differences are statistically significant (Fig. 5 legend). Last, about 50% of the IU1807 chains (≈12% of the total cells) contained one or two larger, more spherical, irregular cells (Fig. 4B and 5, bar 6), in contrast to the uniformly shaped IU1744 cells (Fig. 3B). Thus, moderate PcsB underexpression led to different cell shapes and chain formation in the R6 and D39 backgrounds.

R6 and D39 contain numerous genetic differences, including a Δ*cps* (capsule biosynthesis) mutation in R6 (33). Therefore, we tested whether capsule (or its biosynthesis) contributed to the differences in shape and chain formation of D39 compared

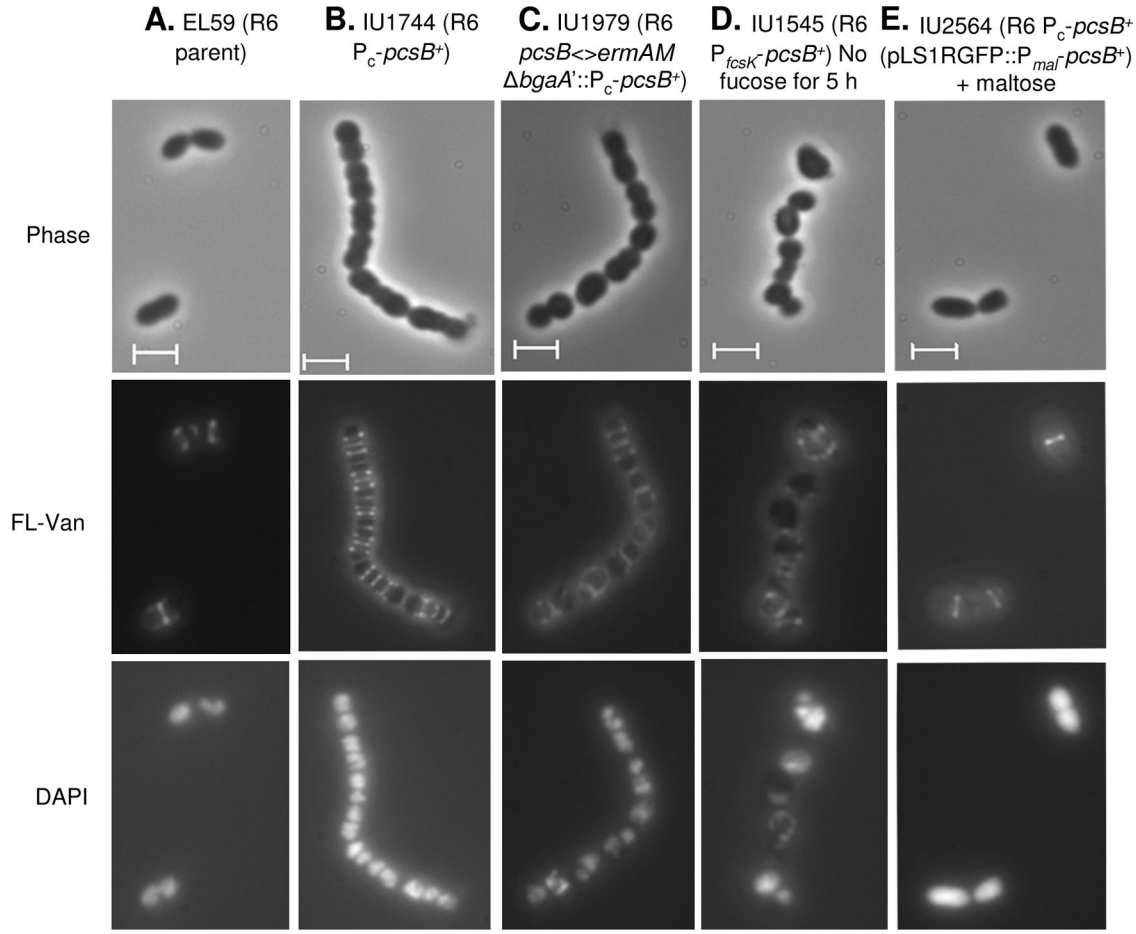

FIG. 3. Representative micrographs of R6-derived strains expressing various amounts of PcsB. See Table 2 for relative expression levels. Phase-contrast microscopy and staining with FL-Van and DAPI are described in Materials and Methods. Bar, 2 μm. (A, B, C, and E) Cells from cultures growing exponentially in BHI broth at 37°C (with 1% [wt/vol] maltose for panel E); (D) a culture depleted of PcsB for 5 h by removal of fucose. See the text for additional details.

to R6 when PcsB was moderately underexpressed. An isogenic D39 Δ*cps* mutant (IU1945 [Table 1]), which contained the same deletion in the *cps* region as R6 (33), formed primarily diplococci or short chains of cells compared to D39 (Fig. 4A and D and 5, bars 4 and 9). This D39 Δ*cps* mutant grew with the same lag and doubling time as the D39 parent strain (data not shown), in contrast to some other Δ*cps* mutants, which were reported to show longer lags under different culture conditions than those used here (4). Unexpectedly, cells of this unencapsulated mutant were significantly less ovoid (AR, 1.32) than those of the D39 parent (AR, 1.69) (Fig. 5, bars 4 and 9). This change in cell shape was confirmed by a second, independent unencapsulated mutant (IU3192 [Table 1]) (Fig. 5, bar 8) but was not observed in the nonisogenic R6 background (Fig. 5, bar 1). Thus, encapsulated D39 formed longer chains of more ovoid-shaped cells than isogenic unencapsulated mutants.

When PcsB was moderately underexpressed in the D39 Δ*cps* mutant (IU2336 [Table 1]) to approximately the same level as in the encapsulated D39 IU1807 mutant (Table 2), the cells became more spherical (AR, 1.14) and formed longer chains than cells of the D39 Δ*cps* parent, IU1945 (Fig. 4E and 5, bars 9 and 10). These shape and chain formation phenotypes were similar to those of the unencapsulated R6 mutants underexpressing PcsB to about the same levels as IU2336 (Table 2; Fig. 3 and 5). Notably, the shape and chain formation properties of the D39 Δ*cps* mutant moderately underexpressing PcsB (IU2336) (Fig. 4E and 5, bar 10) were substantially different from those of the corresponding isogenic D39 *cps*$^+$ strain (IU1807) (Fig. 4B and 5, bars 5 and 6); so much so that the strains could be distinguished based on phase microscopy. As confirmation, we obtained the same cell shape and chain formation properties when PcsB was moderately underexpressed in an independently constructed D39 Δ*cps* mutant (data not shown). Thus, the cell shape and chain formation of the D39 parent and *pcsB* mutants were influenced by the presence or biosynthesis of capsule, but in the absence of capsule, moderate PcsB underexpression caused similar morphology changes in the R6 and D39 backgrounds.

Finally, severe underexpression of PcsB to barely detectable levels in D39 strain IU2537 (Δ*pcsB*<>*ermAM* Δ*bgaA*'::P_c-*pcsB*$^+$ [Table 2]) or deprivation of PcsB in D39 strain IU2091 (P_{fcsK}-*pcsB*$^+$ [native locus] lacking fucose [Table 2]) resulted in the formation of chains of irregular, sometimes enlarged, spherical

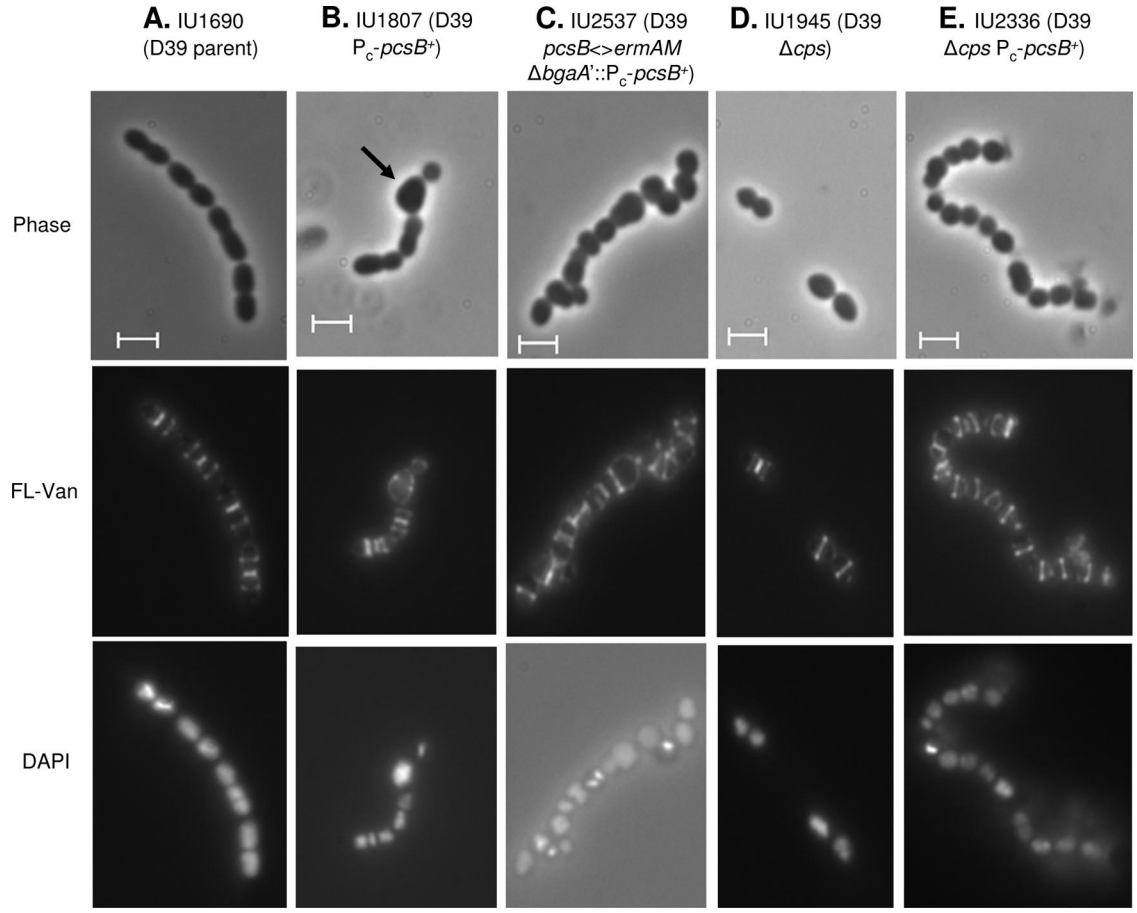

FIG. 4. Representative micrographs of D39-derived strains growing exponentially in BHI broth at 37°C and expressing various amounts of PcsB. See Table 2 for relative expression levels. Phase-contrast microscopy and staining with FL-Van and DAPI are described in Materials and Methods. Bar, 2 μm. The arrow in panel B indicates a typical large, more spherical cell formed in strain IU1807. See the text for additional details.

cells (Fig. 4C and 5, bar 7, and data not shown), similar to those of R6 strain IU1545 depleted for PcsB (Fig. 3D). PcsB expression was likely lower in strains IU2091 and IU1545 lacking fucose than in IU2537, because IU2091 and IU1545 stopped growing, formed mainly diplococci or short chains of cells, and aggregated into clumps (data not shown), whereas, IU2537 did grow (see Fig. S1 in the supplemental material), still formed longer chains (Fig. 5, bar 6), and did not aggregate (data not shown). These exaggerated phenotypes were again ascribable to PcsB underexpression and not decreased MreCD expression, because repair (knock-in) of the *mreCD*$^+$ Δ*pcsB*<>*ermAM* allele in strain IU2537 (Fig. 4C) with a Δ*mreCD*<>Spec^r *pcsB*$^+$ allele restored wild-type D39 cell morphology (data not shown). Thus, severe underexpression or prolonged depletion of PcsB led to the formation of similar short chains of irregular, enlarged spherical cells in both the R6 and D39 backgrounds.

Capsule influences the chain formation and division of other PG biosynthesis mutants. We tested whether capsule affected the morphology of other cell shape and chain formation mutants of *S. pneumoniae.* An unencapsulated D39 Δ*cps* Δ*dacA* mutant, which lacked the D,D-carboxypeptidase that cleaves the ultimate D-Ala from stem peptides (28, 44, 59, 70), formed a greater number of chains (≈47%) containing more spherical cells (AR, 1.1) (Fig. 6B) than its largely diplococcal, semiovoid D39 Δ*cps* parent (Fig. 4D and 5, bar 9). These shape and chain formation phenotypes paralleled those of unencapsulated strains moderately underexpressing PcsB described above. D39 Δ*cps* Δ*dacA* mutant cells accumulated D-Ala-D-Ala in their PG, which caused pronounced uniform staining of entire cell surfaces with FL-Van (Fig. 6). Most D39 Δ*cps* Δ*dacA* cells contained one equatorial ring, and DAPI staining indicated diffuse nucleoids occupying entire cells (Fig. 6B). In addition, about 18% of the D39 Δ*cps* Δ*dacA* cells contained multiple or nonparallel equatorial rings (Fig. 6B). In contrast, an encapsulated D39 Δ*dacA* mutant (Fig. 6A) formed a much higher proportion of diplococci (40%) compared to its D39 parent, which mainly formed medium-length (11 ± 1 cell) chains (Fig. 4A and 5, bar 4). This behavior again paralleled moderate PcsB underexpression in the encapsulated strain (Fig. 5, bar 5). However, D39 Δ*dacA* cells were far more spherical (AR, 1.1) (Fig. 6A) than ovoid D39 (AR, 1.69) (Fig. 4A) or IU1807 (AR, 1.47) (Fig. 4B) cells. There were also fewer (≈4%) cells containing misplaced or multiple equatorial rings in the encapsulated compared to the unencapsulated Δ*dacA* mutant (Fig. 6A and B), although all Δ*dacA* mutants tended to aggregate in culture.

We observed a similar effect of capsule on the chain formation pattern of a Δ*lytB* mutant. *lytB* encodes a glucosaminidase

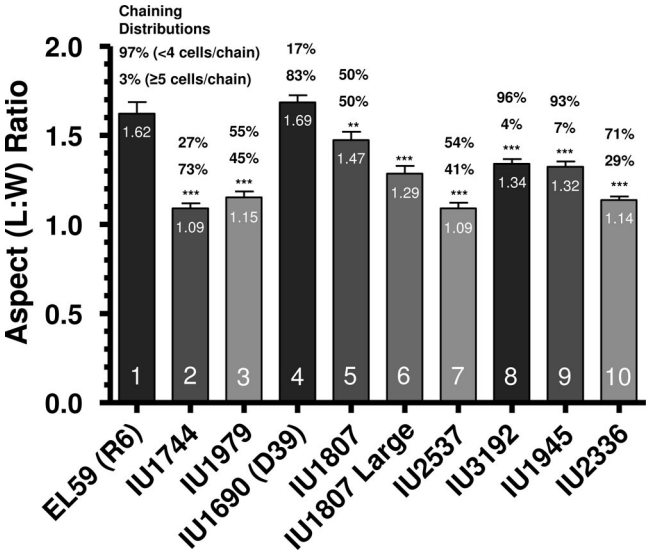

FIG. 5. Length-to-width ARs and chain formation distributions of R6- and D39-derived strains expressing various amounts of PcsB growing exponentially in BHI broth at 37°C. Phase-contrast microscopy and determinations of ARs from micrographs, such as those in Fig. 3 and 4, were performed as described in Materials and Methods. Average ARs (listed at tops of bars) were based on ≈25 individual cells from multiple independent cultures (usually ≥3). Standard errors of the mean ARs are indicated. ***, $P < 0.0001$; **, $P < 0.005$, determined by two-tailed *t* tests relative to the following parent strains: bars 2 and 3 versus 1; bars 5 to 9 versus 4, and bar 10 versus 9. The chain formation distributions of strains are indicated above the bars and are based on ≈100 separate chains of cells from multiple independent cultures (usually ≥3). The upper and lower numbers correspond to the percentage of chains that contain two (diplococcus) or four cells and chains that contain greater than five cells, respectively. The average chain lengths for R6 (bar 1) and D39 (bar 4) were 2.5 ± 0.1 and 11 ± 1 cells per chain, respectively. 1807 Large refers to the larger cells in chains of strain IU1807. See text for additional details.

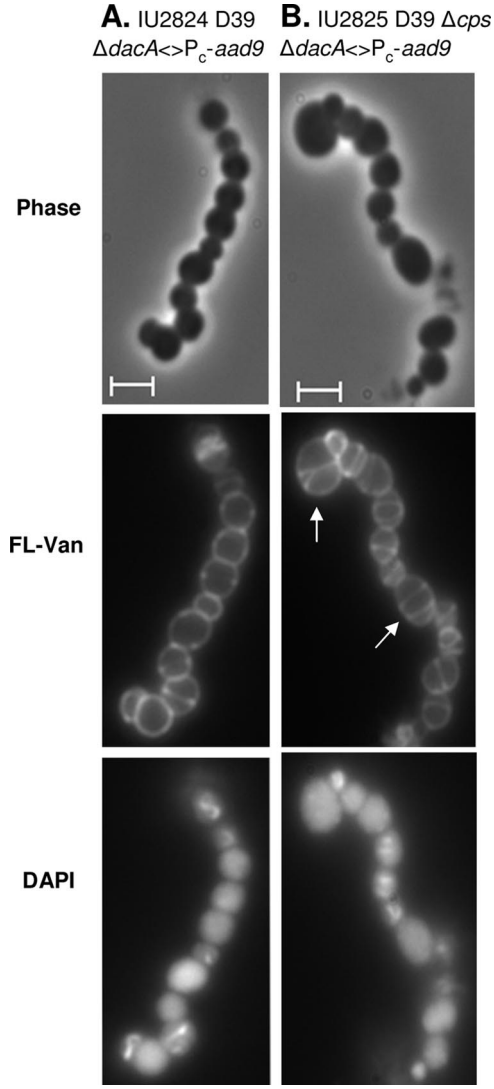

FIG. 6. Representative micrographs of encapsulated D39 Δ*dacA* and isogenic unencapsulated D39 Δ*cps* Δ*dacA* growing exponentially in BHI broth at 37°C. Phase-contrast microscopy and staining with FL-Van and DAPI are described in Materials and Methods. Bar, 2 μm. The arrows in panel B indicate typical cells containing multiple or misplaced equatorial rings in strain IU2825. See text for additional details.

that cleaves the murein glycan chain and participates in a late step in cell separation (14, 27). *lytB* mutants were reported to form long chains of normally shaped cells in the R6 background (14). Similar to R6, introduction of a Δ*lytB*::P_c-*ermAM* mutation into unencapsulated D39 Δ*cps* (IU1945) caused cells to go from diplococci and short chains of four cells (Fig. 5, bar 9) to long chains (strain IU2988) (data not shown). In contrast, the D39 Δ*lytB*::P_c-*ermAM* mutant (IU2898) formed only moderately longer chains than its D39 parent (data not shown). Together, these results show that the absence of capsule allowed chain formation to occur for the *pcsB*, Δ*dacA*, and Δ*lytB* mutants, and capsule (or its biosynthesis) influenced the cell shape of *pcsB* and equatorial ring placement in Δ*dacA* mutants (Fig. 3 to 6).

Cell defects caused by PcsB underexpression are not correlated with changes in the composition of peptides in PG, which is significantly different in strains R6 and D39. Unpublished experiments indicated that the composition of PG peptides was unchanged in a Δ*pcsB* mutant of *S. agalactiae* (55). On the other hand, absence of the CHAP domain-containing Sle1 amidase changed the composition of the PG peptides in *S. aureus* (32). Therefore, we determined whether PcsB underexpression or the absence of MreCD affected the composition of the PG peptides in this set of serotype 2-derived strains. Building on pioneering work of Tomasz and colleagues (25, 26, 60, 61, 63), we purified PG from parent and isogenic mutant strains, hydrolyzed off lactoyl-peptides with base and resolved the lactoyl-peptide peaks by RP-HPLC (see Materials and Methods) (2). Unlike previously validated procedures (26, 61, 63), this method does not require the use of a purified amidase. Typical chromatograms for parent strains R6 and D39 appear in Fig. 7, and validation of these methods in pneumococcus is described in Materials and Methods. Each peak was collected, and lactoyl-peptides were identified by mass spectrometry (see Materials and Methods and and the supplemental material). Consistent with previous reports (25, 60, 61), there was a striking difference in the lactoyl-peptide compositions of laboratory strain R6 and virulent strain D39 (Fig. 7; see also Table S2 in

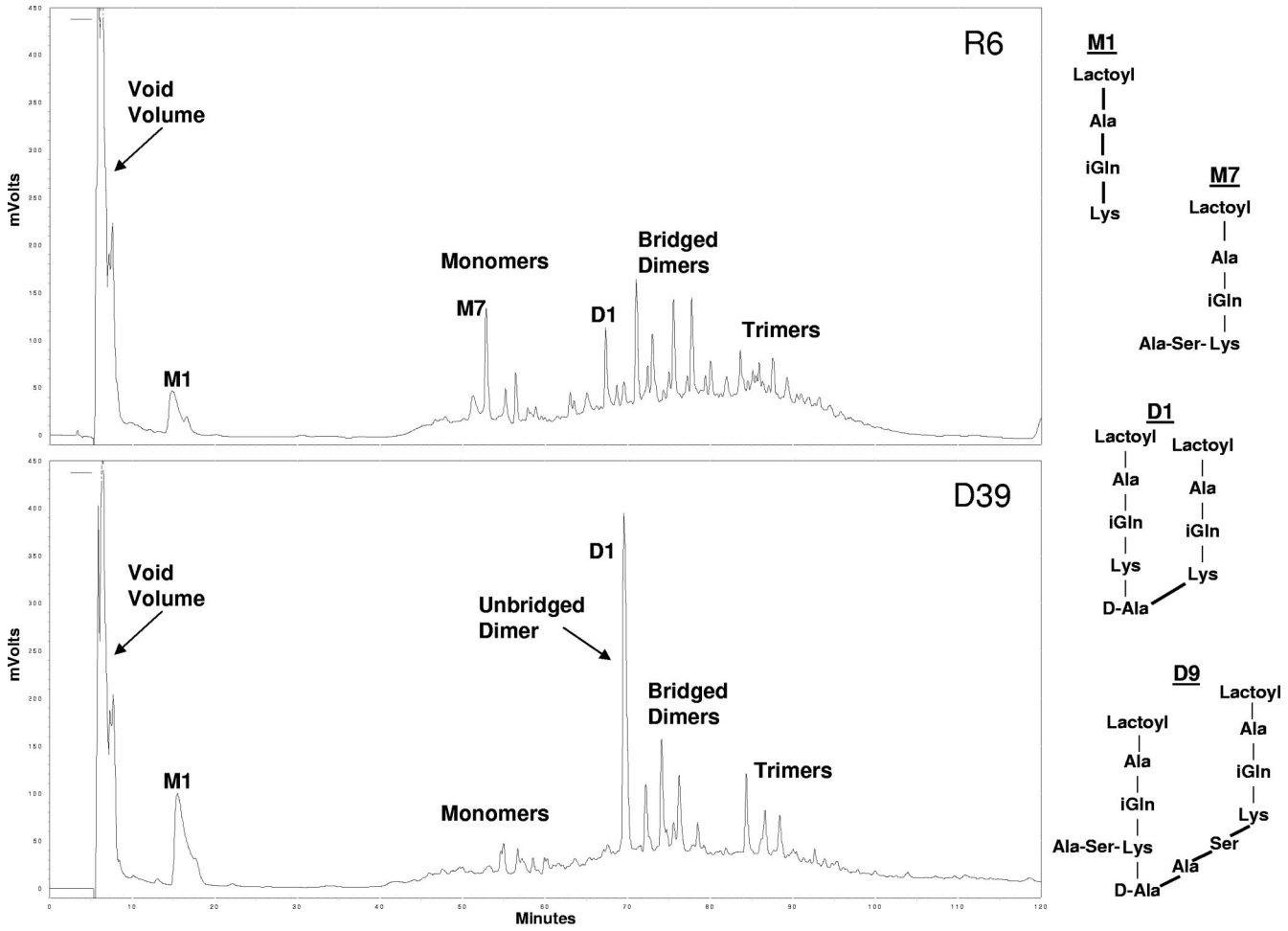

FIG. 7. Lactoyl-peptide compositions of strains R6 (top) and D39 (bottom). PG was isolated from cells growing exponentially in BHI broth at 37°C, lactoyl-peptides were released by base hydrolysis, and RP-HPLC was performed as described in Materials and Methods. The total yields of all lactoyl-peptides were similar for the unencapsulated R6 and encapsulated D39 strains (2.9×10^7 and 3.3×10^7 arbitrary mvolt area units, respectively). The structures of the lactoyl-peptides in each peak were determined by MS, and representative structures of species containing (monomer M7 and dimer D9) or lacking (monomer M1 and dimer D1) Ala-Ser additions and cross-bridges are shown. Complete peak assignments and other lactoyl-peptide structures are provided in the supplemental material. Quantitation of the relative amounts of each lactoyl-peptide from the R6 and D39 chromatograms can be found in Table S2 of the supplemental material. Underexpression or severe depletion of PcsB or the absence of MreCD did not affect the relative amounts or composition of the lactoyl-peptides, and the same chromatogram was obtained for unencapsulated strain D39 Δ*cps* as shown for its encapsulated parent D39 (see text).

the supplemental material). The PG of R6 contained monomer stem peptides with Ala-Ser and Ala-Ala additions on Lys (e.g., M7) (Fig. 7) and a significant number of cross-linked dimer peptides with Ala-Ser and Ala-Ala cross-bridges (e.g., D9) (Fig. 7). In contrast, D39 PG lacked monomer peptides containing Ala-Ala and Ala-Ser additions and mainly contained dimers lacking Ala-Ser and Ala-Ala cross-bridges (e.g., D1) (Fig. 7). The MurMN ligases catalyze Ala-Ser and Ala-Ala addition (19, 24, 63). We rechecked the sequences of *murMN* in both strains, and they were the same, as expected from a previous genome comparison (33). Control experiments showed that the D39 Δ*cps* mutant produced the same lactoyl-peptide chromatogram as parent strain D39, indicating that capsule was not the source of this difference between D39 and R6 (data not shown). The basis for this difference is considered in the Discussion.

The PG peptide profiles were determined for *pcsB* mutants underexpressing PcsB to various levels (Table 2) and in R6 overexpressing PcsB from plasmid pLS1RGFP::P_{mal}-*pcsB*$^+$ (Table 2). The relative amount of each lactoyl-peptide within a PG preparation did not change upon PcsB underexpression or moderate overexpression compared to that of the *pcsB*$^+$ parent (data not shown). In addition, there was no correlation between the severity of cell morphology defects (Fig. 3 and 4) and the relative composition of PG peptides in either the R6 or D39 backgrounds, even for cells depleted of PcsB for 5 h (data not shown). Moreover, no statistically significant changes were detected in the absolute amounts or recovery of individual lactoyl-peptides between the parent and *pcsB*-underexpressing strains harvested at similar cell densities (data not shown) (see Materials and Methods). Finally, the Δ*mreCD* mutant did not affect the relative lactoyl-peptide composition or amounts in the R6 background (data not shown).

PcsB underexpression is not correlated with penicillin sensitivity. We reported previously that some strains underex-

pressing PcsB appeared to be more sensitive to penicillin G, although penicillin sensitivity did not seem to be simply correlated with PcsB expression (45). Recently, it was reported that Δ*pcsB* mutants had increased sensitivity to penicillin G in some serotypes of *S. pneumoniae* (29). Therefore, we repeated sensitivity tests in unencapsulated R6 strains expressing different amounts of PcsB in BHI broth. Strain IU1979, which expressed only ≈14% of the wild-type level of PcsB (Table 2) and showed cell division defects (Fig. 3C), had the same sensitivity to 0.01 μg and 0.1 μg penicillin G per ml as parent strains R6 and IU1533 (Table 1 and data not shown). Therefore, penicillin sensitivity was not correlated with PcsB underexpression.

Underexpression of PcsB induces expression of the VicRK regulon. We performed microarray experiments to determine how *S. pneumoniae* deals with the defective cell division caused by PcsB underexpression. Strains IU1979 (Δ*pcsB*<>*ermAM* Δ*bgaA′*::P_c-*pcsB*$^+$; ≈14% relative PcsB amount) and isogenic control strain IU1533 (*pcsB*$^+$ Δ*bgaA*'::P_c-*pcsB*$^+$; similar PcsB amount as R6 [data not shown]), were grown exponentially in BHI broth (see Fig. S2 in the supplemental material). RNA was extracted and microarray analyses were performed as described in Materials and Methods. The largest increases in relative transcript amounts were confined to other members of the VicRK regulon (43, 46, 47), including *spr0096*, *lytB* (*spr0867*), and *spr1875* (Table 3). The relative increase in *lytB* transcript amount was accompanied by a trend back to shorter chains (Fig. 5, bar 3), consistent with the role of LytB as an acetylglucosaminidase (14). Besides the VicRK regulon, changes in relative transcript amounts were surprisingly limited, given the extreme defect in cell shape and morphology (Fig. 3). These other changes included some small increases in the relative transcript amounts of stress-mediating genes, such as *clpL*, *groEL*, and *groES* (Table 3).

Notably, the relative amounts of the *mreC* and *mreD* transcripts did not change in the Δ*pcsB*<>*ermAM* mutant (IU1979) compared to the *pcsB*$^+$ control (IU1533), consistent with the minimal changes detected in relative MreC amount (Table 2). Finally, the relative amount of *pcsB* transcript detected in the microarray analysis did not appear lower in the strain underexpressing PcsB protein (IU1979) (Table 2). Additional characterization of these strains by QPCR showed that this apparent discrepancy was likely caused by changes in differential stability of the *pcsB-bgaA′* fusion transcript produced from the ectopic Δ*bgaA′*::P_c-*pcsB*$^+$ site (Fig. 1B). The amounts of the *pcsB* transcript corresponding to promoter-proximal (5′) regions of the fusion transcript were significantly lower than those from the corresponding segments of the native *pcsB*$^+$ transcript (data not shown), which would reduce the relative amount of PcsB protein produced in the ectopic fusion strain. At the same time, the amount of the promoter-distal (3′) segment of the *pcsB* fusion transcript corresponding to the oligonucleotide probe on the microarray remained similar to that of the wild-type transcript.

TABLE 3. Changes in relative transcript amounts caused by PcsB underexpression in strain IU1979 compared to isogenic strain IU1533 growing exponentially in BHI broth at 37°C[a]

Effect on expression and gene tag	Function[b]	Fold change[c]	Bayesian *P* value[c]
Decreased relative expression			
spr0088	Hypothetical protein	−1.9	5.6E-04
spr0128	Hypothetical protein	−1.9	1.6E-04
spr0446	*hsdS*; type I restriction enzyme EcoKI specificity protein (S protein)	−2.4	2.9E-05
spr0504	*licT*; transcriptional anti-terminator (BglG family)	−1.9	2.1E-04
spr0505	*pts-eii*; phosphotransferase system sugar-specific EII component	−2.0	1.4E-04
spr0506	*bglH*; 6-phospho-beta-glucosidase	−1.9	1.9E-04
spr0778	*fruR*; transcriptional repressor of the fructose operon	−1.9	5.3E-03
spr0779	*fruB*; fructose-1-phosphate kinase	−2.1	1.5E-03
spr0780	*fruA*; fructose specific-phosphotransferase system IIBC component	−2.2	1.4E-03
Increased relative expression			
spr0096	**Hypothetical protein**	**4.1**	**1.2E-06**
spr0307	*clpL*; ATP-dependent protease ATP-binding subunit	2.6	3.5E-07
spr0445	*hsdS*; type I restriction enzyme	3.4	9.0E-07
spr0565	*bgaA*; β-galactosidase precursor	2.4	4.1E-05
spr0867	***lytB*; Endo-β-*N*-acetylglucosaminidase**	**2.7**	**6.6E-07**
spr1016	Hypothetical protein	2.0	7.5E-05
spr1601	Hypothetical protein	1.9	1.6E-05
spr1722	*groEL*; chaperonin GroEL	2.3	3.7E-05
spr1723	*groES*; co-chaperonin GroES	2.3	1.4E-06
spr1872	*pcp*-truncation; pyrrolidone carboxyl peptidase, truncation	1.9	4.8E-05
spr1873	Conserved hypothetical protein	2.4	3.3E-06
spr1874	***marR*; transcriptional regulator, MarR family**	**3.3**	**1.2E-06**
spr1875	**Conserved hypothetical protein**	**7.9**	**3.9E-09**

[a] IU1533 (R6 *pcsB*$^+$ Δ*bgaA′*::P_c-*pcsB*$^+$) was used as the parent strain instead of R6 to control for insertion into the *bgaA* locus required to construct PcsB-underexpressing strain IU1979 (Δ*pcsB*<>*ermAM* Δ*bgaA′*::P_c-*pcsB*$^+$). Representative growth curves from these experiments are shown in Fig. S2 of the supplemental material.

[b] Members of the VicRK regulon are shown in bold type.

[c] Microarray analyses were performed as described in Materials and Methods. The data set includes four biological replicates, including two dye swaps, with final cutoff values of <1.8 for fold changes and $P < 0.005$.

DISCUSSION

Characterization of cell shape and chain formation phenotypes caused by PcsB underexpression initially suggested differences between laboratory strain R6 and virulent serotype 2 strain D39 (Fig. 3 and 4). Moderate underexpression of PcsB in diplococcal R6 (Table 2) led to the formation of chains, and cells became more spherical than the ovoid R6 parent strain (Fig. 3A, B, and C; Fig. 5, bars 1 to 3). In contrast, similar PcsB underexpression in D39 (Table 2) led to the appearance of diplococci and shorter chains and caused a far smaller decrease in AR than in R6 (Fig. 5, bars 4 and 5). In addition, about 12% of the D39 *pcsB* mutant cells were large, spherical, and irregularly shaped (Fig. 4B and 5, bar 6). To determine whether this difference in response to moderate PcsB underexpression in R6 and D39 was due to the presence or biosynthesis of capsule, we compared the shape and chain formation of D39 with an isogenic D39 Δ*cps* unencapsulated mutant. Cells of unencapsulated mutants of D39 formed diplococci instead of medium-length chains and, unexpectedly, were less ovoid than the cells

of the D39 parent strain (Fig. 4A and D and 5, bars 4, 8, and 9). Moderate underexpression of PcsB in the D39 Δ*cps* mutant (Table 2) caused formation of chains and more spherical cells compared to the D39 Δ*cps* strain (Fig. 4D and E and 5, bars 9 and 10), similar in appearance to those seen in R6 (Fig. 3B and C and 5, bars 2 and 3). However, the shape and chain formation properties of the D39 Δ*cps* mutant moderately underexpressing PcsB (Fig. 4E and 5, bar 10) were substantially different from those of the corresponding isogenic D39 *cps*$^+$ strain (Fig. 4B and 5, bars 5 and 6). Finally, severe underexpression or depletion of PcsB (Table 2) led to the formation of short chains of highly distended, spherical cells with aberrantly placed division junctions in both the R6 and D39 backgrounds (Fig. 3D, 4C, and 5, bar 7). Together, these results show that capsule caused the formation of chains in D39, and more surprisingly, influenced the cell shape and chain formation phenotypes of the wild-type D39 strain and *pcsB* mutants (see Results).

The masking and modulation of cell chain formation and division phenotypes by capsule extended to other mutants, such as Δ*dacA* (Fig. 6) and Δ*lytB* mutants (see Results). The *pcsB* and *dacA* mutant phenotypes paralleled each other in some ways (see Results). In serotype 2 *S. pneumoniae*, the capsule is covalently linked to PG (reviewed in references 49 and 69). Capsule negatively influences the spontaneous and antibiotic-induced autolysis of *S. pneumoniae* strains monitored by optical density (23), which we confirmed for D39 (data not shown). This autolysis is largely mediated by the LytA amidase (23). The effects of capsule on cell shape presented here and on LytA-mediated autolysis could indicate that the capsular polysaccharide acts as a considerable physical barrier or guide in cell division. On the other hand, there might be metabolic communication between the capsule biosynthetic pathway and the cell division and PG biosynthetic machinery. In either case, capsule (or its biosynthesis) can affect the cell shape and chain formation phenotypes of pneumococcal mutant strains deficient in cell division or PG biosynthesis.

The experiments reported here also indicate that the cell defects observed in these mutants is due directly to PcsB underexpression and support the conclusion that *pcsB* is essential in serotype 2 strains. Seemingly benign mutations in the *pcsB* native locus, such as an exact reading frame replacement (Δ*pcsB*<>*ermAM* in a merodiploid strain) (Fig. 1A), led to slightly decreased expression of the upstream MreC protein, especially in D39 (Table 2). Other mutant constructs, such as P_c-pcsB$^+$ and P_{fcsK}-*pcsB*$^+$ insertions in the *pcsB* locus (Fig. 1C), also decreased the MreC amount slightly (Table 2), possibly because these constructs contain an oppositely transcribed *kan* marker. Nevertheless, ectopic expression of just the *pcsB*$^+$ gene from another chromosome location (*bgaA*) or from a plasmid fully complemented the cell shape and chain formation defects caused by PcsB underexpression (Fig. 3 and 4). Furthermore, we were able to delete *mreCD* in serotype 2 *S. pneumoniae*, and these Δ*mreCD* mutants did not interfere with downstream *pcsB* expression (Table 2) or cause defects in cell morphology (data not shown). MreCD are conditionally essential in rod-shaped bacteria, such as *E. coli*, which readily accumulates suppressor mutations when *mreCD* are disrupted (reference 5 and references therein). Additional experiments to be reported elsewhere show that suppressors do not accumulate in these Δ*mreCD* mutants of serotype 2 *S. pneumoniae* (A. D. Land, unpublished results).

Depletion of PcsB for 5 h in encapsulated or unencapsulated mutants resulted in severe cell division defects (Fig. 3 and 4), and these cultures never resumed growth. Moreover, we could not knock out *pcsB* at the native locus without ectopic expression of *pcsB*$^+$ from elsewhere (see Results), and we did not obtain putative suppressors after 3 days of incubation. Together, these observations support the conclusion that *pcsB* is indeed essential in serotype 2 strains. Previously, knockout mutants of the *pcsB* ortholog, *gbpB*, were reported in some strains of *S. mutans* (11), but another study that attempted several gene disruption approaches concluded that *gbpB* was essential in the *S. mutans* strain used (41). Recently, it was reported that Δ*pcsB* mutants could be isolated in serotype 4 and 6B strains; however, these mutants were isolated under selective pressure, and their growth was greatly diminished, even in rich medium (29). Therefore, it is possible that suppressors accumulated in these Δ*pcsB* mutants and that *pcsB* is also essential in these serotype strains. Consistent with this interpretation, we could obtain putative bypass suppressors in a D39 Δ*pcsB* mutant at very low frequency after prolonged incubation for at least 6 days at 37°C (data not shown).

We also used the sets of strains expressing different amounts of PcsB to test other hypotheses about PcsB expression and function. Quantitative Western blotting showed that cell-associated PcsB is moderately abundant and present in ≈4,900 monomers per cell (Fig. 2C; Table 2). This amount is comparable to other cell division proteins, such as FtsZ and FtsA in *S. pneumoniae* (34) and MreC in *B. subtilis* (64), which are present in approximately 3,000, 2,200, and 12,000 molecules per cell, respectively. Despite the relative abundance of cell-associated PcsB, at least an equal amount of PcsB is secreted into the growth medium (Fig. 2A). Since a relatively small drop of three- to fivefold in PcsB amount caused defects in cell division (Table 2; Fig. 3 and 4), the normal amount of PcsB is not present in large excess. All cell-associated and secreted PcsB was processed in strains R6 and D39 (Fig. 2A), which contrasts with a previous report for this genetic background (42). We do not know the reason for this discrepancy, but we confirmed our conclusion by three different approaches, including epitope tagging of PcsB (Fig. 2A). This result suggests that extracellular PcsB and cytoplasmic DivIVA probably do not interact directly (21). We did not find a correlation between PcsB underexpression or the absence of MreCD and increased penicillin sensitivity in unencapsulated strains. However, we did confirm the previous observation (23) that capsule masks penicillin-induced autolysis for encapsulated strain D39 and its derivatives (data not shown). Finally, microarray results presented here indicate that PcsB underexpression and the defective cell division that ensues are likely sensed by the VicRK two-component system, which responds by increasing the relative transcript amounts of other regulon members (Table 3). However, no other large changes in relative gene expression were detected that would provide information about possible signal pathways.

We did not find any change in the relative amounts or composition of the PG peptides in R6 or D39 strains underexpressing or severely depleted for PcsB or with *mreCD* deleted (Fig. 7). However, our analyses did confirm the surprising result that the PG of R6 contained an extensive

number of Ala-Ala and Ala-Ser additions and cross-bridges in its peptide monomers, dimers, and trimers, whereas the PG of D39 largely lacked these additions (Fig. 7; see also Table S2 and other data in the supplemental material). This difference was reported without comment for strains R6 compared to R36A and D39S in earlier work by Tomasz and coworkers (25, 60, 61) (see also Table S2 in the supplemental material). Laboratory strain R6 was derived from unencapsulated strain R36A, which itself was a second derivative of encapsulated strain D39 (33). PG peptides from strain R36A largely lack Ala-Ala and Ala-Ser additions and cross-bridges, like strain D39 (Fig. 7) (25, 60, 61, 63). Therefore, synthesis of these additions must have been acquired during the derivation and storage of the current R6 isolate. Ala-Ala and Ala-Ser additions are synthesized by the MurMN tRNA-dependent ligases (19, 24, 39), and loss of MurMN function has been correlated with loss of antibiotic resistance in some cases (reviewed in reference 63). However, the *murMN* genes are identical in the R6 and D39 strains, and capsule did not cause the different PG compositions of R6 and D39. There are about 80 mutational changes between the genome sequences of R6 and D39 (33), but none appears to affect the amounts or charging of $tRNA^{Ser}$ and $tRNA^{Ala}$, which are substrates for MurMN. Interestingly, some of the mutational differences are in genes that mediate PG metabolism, including *pbp1A*, *murZ* (a paralog of *murA*), *ftsX*, and *dltA* (33). These mutations or others must account for the difference in PG composition between R6 and D39, pointing to an unknown facet of Ala-Ala and Ala-Ser formation in pneumococcal PG. Finally, unencapsulated R6 and D39 Δ*cps* were equally sensitive to penicillin G (data not shown), despite their different PG compositions (Fig. 7). This result supports the previous conclusion that the extent of Ala-Ala and Ala-Ser addition and cross-bridge formation is not strictly correlated with resistance to β-lactam antibiotics (63).

The HPLC methods used to determine PG peptide composition (Fig. 7) were modified to assay for amidase and endopeptidase activity of purified preparations of PcsB, such as the PcsB-(C)-His_6 used as a standard in Fig. 2C (L.-T. Sham, unpublished result). To date, we have been unable to detect murein hydrolase activity in reaction mixtures similar to those used to assay Sle1 (32) for several PcsB constructs, which are monomers in solution (L.-T. Sham, unpublished result). Likewise, other attempts to detect murein hydrolase activity of purified PcsB and its homolog have not been successful (29, 41, 56, 67). The lack of changes in PG peptide composition in cells severely depleted for PcsB whose morphology is strongly affected (Fig. 3, 4, and 7) argues against PcsB acting as a major murein hydrolase or autolysin. It is still possible that PcsB might act as a weak murein hydrolase at specific times in cell division or on rare PG peptide species that are not detected in these assays. It is also possible that purified PcsB needs to interact with another protein for hydrolase activity. On the other hand, the new results presented here, including its relative abundance, and those reported previously (29, 41, 45, 56) are consistent with PcsB acting as a scaffolding protein. This important issue remains to be resolved.

ACKNOWLEDGMENTS

We thank Krystyna Kazmierczak and Kelli Gibson for constructing some strains used in this study, Krystyna Kazmierczak and Kyle Wayne for helpful discussions, Alina Gutu for help with protein purifications, Donald Morrison for CSP-1 and bacterial strains, Paloma Lopez for plasmid pLS1RGFP, Lilly Research Labs for strains EL59 and EL1454, and the National Center for Glycomics and Glycoproteomics at Indiana University Bloomington for access to their mass spectrometry facility.

This work was funded by grant 0543289 from the National Science Foundation and grant AI060744 from the National Institute of Allergy and Infectious Diseases to M.E.W. and NIH grant 5P41RR018942 to the National Center for Glycomics and Glycoproteomics. S.M.B. was a predoctoral trainee on NIH grant F31FM082090.

The contents of this report are solely the responsibility of the authors and do not necessarily represent the official views of the National Science Foundation, NIAID, or NIH.

REFERENCES

1. **Anantharaman, V., and L. Aravind.** 2003. Evolutionary history, structural features and biochemical diversity of the NlpC/P60 superfamily of enzymes. Genome Biol. **4:**R11.
2. **Arbeloa, A., J. E. Hugonnet, A. C. Sentilhes, N. Josseaume, L. Dubost, C. Monsempes, D. Blanot, J. P. Brouard, and M. Arthur.** 2004. Synthesis of mosaic peptidoglycan cross-bridges by hybrid peptidoglycan assembly pathways in gram-positive bacteria. J. Biol. Chem. **279:**41546–41556.
3. **Bateman, A., and N. D. Rawlings.** 2003. The CHAP domain: a large family of amidases including GSP amidase and peptidoglycan hydrolases. Trends Biochem. Sci. **28:**234–237.
4. **Battig, P., and K. Muhlemann.** 2007. Capsule genes of *Streptococcus pneumoniae* influence growth *in vitro*. FEMS Immunol. Med. Microbiol. **50:**324–329.
5. **Bendezu, F. O., and P. A. de Boer.** 2008. Conditional lethality, division defects, membrane involution, and endocytosis in *mre* and *mrd* shape mutants of *Escherichia coli*. J. Bacteriol. **190:**1792–1811.
6. **Billot-Klein, D., R. Legrand, B. Schoot, J. van Heijenoort, and L. Gutmann.** 1997. Peptidoglycan structure of *Lactobacillus casei*, a species highly resistant to glycopeptide antibiotics. J. Bacteriol. **179:**6208–6212.
7. **Billot-Klein, D., D. Shlaes, D. Bryant, D. Bell, J. van Heijenoort, and L. Gutmann.** 1996. Peptidoglycan structure of *Enterococcus faecium* expressing vancomycin resistance of the VanB type. Biochem. J. **313:**711–715.
8. **Bisicchia, P., D. Noone, E. Lioliou, A. Howell, S. Quigley, T. Jensen, H. Jarmer, and K. M. Devine.** 2007. The essential YycFG two-component system controls cell wall metabolism in *Bacillus subtilis*. Mol. Microbiol. **65:**180–200.
9. **Burnaugh, A. M., L. J. Frantz, and S. J. King.** 2008. Growth of *Streptococcus pneumoniae* on human glycoconjugates is dependent upon the sequential activity of bacterial exoglycosidases. J. Bacteriol. **190:**221–230.
10. **Chan, P. F., K. M. O'Dwyer, L. M. Palmer, J. D. Ambrad, K. A. Ingraham, C. So, M. A. Lonetto, S. Biswas, M. Rosenberg, D. J. Holmes, and M. Zalacain.** 2003. Characterization of a novel fucose-regulated promoter (P_{fcsK}) suitable for gene essentiality and antibacterial mode-of-action studies in *Streptococcus pneumoniae*. J. Bacteriol. **185:**2051–2058.
11. **Chia, J. S., L. Y. Chang, C. T. Shun, Y. Y. Chang, Y. G. Tsay, and J. Y. Chen.** 2001. A 60-kilodalton immunodominant glycoprotein is essential for cell wall integrity and the maintenance of cell shape in *Streptococcus mutans*. Infect. Immun. **69:**6987–6998.
12. **Chia, J. S., Y. Y. Lee, P. T. Huang, and J. Y. Chen.** 2001. Identification of stress-responsive genes in *Streptococcus mutans* by differential display reverse transcription-PCR. Infect. Immun. **69:**2493–2501.
13. **Daniel, R. A., and J. Errington.** 2003. Control of cell morphogenesis in bacteria: two distinct ways to make a rod-shaped cell. Cell **113:**767–776.
14. **De Las Rivas, B., J. L. Garcia, R. Lopez, and P. Garcia.** 2002. Purification and polar localization of pneumococcal LytB, a putative endo-beta-*N*-acetylglucosaminidase: the chain-dispersing murein hydrolase. J. Bacteriol. **184:**4988–5000.
15. **den Blaauwen, T., M. A. de Pedro, M. Nguyen-Disteche, and J. A. Ayala.** 2008. Morphogenesis of rod-shaped sacculi. FEMS Microbiol. Rev. **32:**321–344.
16. **Donovan, D. M., J. Foster-Frey, S. Dong, G. M. Rousseau, S. Moineau, and D. G. Pritchard.** 2006. The cell lysis activity of the *Streptococcus agalactiae* bacteriophage B30 endolysin relies on the cysteine, histidine-dependent amidohydrolase/peptidase domain. Appl. Environ. Microbiol. **72:**5108–5112.
17. **Dubrac, S., I. G. Boneca, O. Poupel, and T. Msadek.** 2007. New insights into the WalK/WalR (YycG/YycF) essential signal transduction pathway reveal a major role in controlling cell wall metabolism and biofilm formation in *Staphylococcus aureus*. J. Bacteriol. **189:**8257–8269.
18. **Dubrac, S., P. Bisicchia, K. M. Devine, and T. Msadek.** 2008. A matter of life and death: cell wall homeostasis and the WalKR (YycGF) essential signal transduction pathway. Mol. Microbiol. **70:**1307–1322.
19. **du Plessis, M., E. Bingen, and K. P. Klugman.** 2002. Analysis of penicillin-

binding protein genes of clinical isolates of *Streptococcus pneumoniae* with reduced susceptibility to amoxicillin. Antimicrob. Agents Chemother. **46:** 2349–2357.
20. **Dye, N. A., Z. Pincus, J. A. Theriot, L. Shapiro, and Z. Gitai.** 2005. Two independent spiral structures control cell shape in Caulobacter. Proc. Natl. Acad. Sci. USA **102:**18608–18613.
21. **Fadda, D., A. Santona, V. D'Ulisse, P. Ghelardini, M. G. Ennas, M. B. Whalen, and O. Massidda.** 2007. *Streptococcus pneumoniae* DivIVA: localization and interactions in a MinCD-free context. J. Bacteriol. **189:**1288–1298.
22. **Feng, G., H. C. Tsui, and M. E. Winkler.** 1996. Depletion of the cellular amounts of the MutS and MutH methyl-directed mismatch repair proteins in stationary-phase *Escherichia coli* K-12 cells. J. Bacteriol. **178:**2388–2396.
23. **Fernebro, J., I. Andersson, J. Sublett, E. Morfeldt, R. Novak, E. Tuomanen, S. Normark, and B. H. Normark.** 2004. Capsular expression in *Streptococcus pneumoniae* negatively affects spontaneous and antibiotic-induced lysis and contributes to antibiotic tolerance. J. Infect. Dis. **189:**328–338.
24. **Filipe, S. R., M. G. Pinho, and A. Tomasz.** 2000. Characterization of the *murMN* operon involved in the synthesis of branched peptidoglycan peptides in *Streptococcus pneumoniae*. J. Biol. Chem. **275:**27768–27774.
25. **Garcia-Bustos, J., and A. Tomasz.** 1990. A biological price of antibiotic resistance: major changes in the peptidoglycan structure of penicillin-resistant pneumococci. Proc. Natl. Acad. Sci. USA **87:**5415–5419.
26. **Garcia-Bustos, J. F., B. T. Chait, and A. Tomasz.** 1987. Structure of the peptide network of pneumococcal peptidoglycan. J. Biol. Chem. **262:**15400–15405.
27. **Garcia, P., M. P. Gonzalez, E. Garcia, R. Lopez, and J. L. Garcia.** 1999. LytB, a novel pneumococcal murein hydrolase essential for cell separation. Mol. Microbiol. **31:**1275–1281.
28. **Ghosh, A. S., C. Chowdhury, and D. E. Nelson.** 2008. Physiological functions of D-alanine carboxypeptidases in *Escherichia coli*. Trends Microbiol. **16:** 309–317.
29. **Giefing, C., A. L. Meinke, M. Hanner, T. Henics, M. D. Bui, D. Gelbmann, U. Lundberg, B. M. Senn, M. Schunn, A. Habel, B. Henriques-Normark, A. Ortqvist, M. Kalin, A. von Gabain, and E. Nagy.** 2008. Discovery of a novel class of highly conserved vaccine antigens using genomic scale antigenic fingerprinting of pneumococcus with human antibodies. J. Exp. Med. **205:** 117–131.
30. **Higgins, M. L., and G. D. Shockman.** 1976. Study of cycle of cell wall assembly in *Streptococcus faecalis* by three-dimensional reconstructions of thin sections of cells. J. Bacteriol. **127:**1346–1358.
31. **Howell, A., S. Dubrac, K. K. Andersen, D. Noone, J. Fert, T. Msadek, and K. Devine.** 2003. Genes controlled by the essential YycG/YycF two-component system of *Bacillus subtilis* revealed through a novel hybrid regulator approach. Mol. Microbiol. **49:**1639–1655.
32. **Kajimura, J., T. Fujiwara, S. Yamada, Y. Suzawa, T. Nishida, Y. Oyamada, I. Hayashi, J. Yamagishi, H. Komatsuzawa, and M. Sugai.** 2005. Identification and molecular characterization of an N-acetylmuramyl-L-alanine amidase Sle1 involved in cell separation of *Staphylococcus aureus*. Mol. Microbiol. **58:**1087–1101.
33. **Lanie, J. A., W. L. Ng, K. M. Kazmierczak, T. M. Andrzejewski, T. M. Davidsen, K. J. Wayne, H. Tettelin, J. I. Glass, and M. E. Winkler.** 2007. Genome sequence of Avery's virulent serotype 2 strain D39 of *Streptococcus pneumoniae* and comparison with that of unencapsulated laboratory strain R6. J. Bacteriol. **189:**38–51.
34. **Lara, B., A. I. Rico, S. Petruzzelli, A. Santona, J. Dumas, J. Biton, M. Vicente, J. Mingorance, and O. Massidda.** 2005. Cell division in cocci: localization and properties of the *Streptococcus pneumoniae* FtsA protein. Mol. Microbiol. **55:**699–711.
35. **Layec, S., B. Decaris, and N. Leblond-Bourget.** 2008. Characterization of proteins belonging to the CHAP-related superfamily within the Firmicutes. J. Mol. Microbiol. Biotechnol. **14:**31–40.
36. **Leaver, M., and J. Errington.** 2005. Roles for MreC and MreD proteins in helical growth of the cylindrical cell wall in *Bacillus subtilis*. Mol. Microbiol. **57:**1196–1209.
37. **Lee, M. S., and D. A. Morrison.** 1999. Identification of a new regulator in *Streptococcus pneumoniae* linking quorum sensing to competence for genetic transformation. J. Bacteriol. **181:**5004–5016.
38. **Lleo, M. M., P. Canepari, and G. Satta.** 1990. Bacterial cell shape regulation: testing of additional predictions unique to the two-competing-sites model for peptidoglycan assembly and isolation of conditional rod-shaped mutants from some wild-type cocci. J. Bacteriol. **172:**3758–3771.
39. **Lloyd, A. J., A. M. Gilbey, A. M. Blewett, G. De Pascale, A. El Zoeiby, R. C. Levesque, A. C. Catherwood, A. Tomasz, T. D. Bugg, D. I. Roper, and C. G. Dowson.** 2008. Characterization of tRNA-dependent peptide bond formation by MurM in the synthesis of *Streptococcus pneumoniae* peptidoglycan. J. Biol. Chem. **283:**6402–6417.
40. **Mattos-Graner, R. O., S. Jin, W. F. King, T. Chen, D. J. Smith, and M. J. Duncan.** 2001. Cloning of the *Streptococcus mutans* gene encoding glucan binding protein B and analysis of genetic diversity and protein production in clinical isolates. Infect. Immun. **69:**6931–6941.
41. **Mattos-Graner, R. O., K. A. Porter, D. J. Smith, Y. Hosogi, and M. J. Duncan.** 2006. Functional analysis of glucan binding protein B from *Streptococcus mutans*. J. Bacteriol. **188:**3813–3825.
42. **Mills, M. F., M. E. Marquart, and L. S. McDaniel.** 2007. Localization of PcsB of *Streptococcus pneumoniae* and its differential expression in response to stress. J. Bacteriol. **189:**4544–4546.
43. **Mohedano, M. L., K. Overweg, A. de la Fuente, M. Reuter, S. Altabe, F. Mulholland, D. de Mendoza, P. Lopez, and J. M. Wells.** 2005. Evidence that the essential response regulator YycF in *Streptococcus pneumoniae* modulates expression of fatty acid biosynthesis genes and alters membrane composition. J. Bacteriol. **187:**2357–2367.
44. **Morlot, C., M. Noirclerc-Savoye, A. Zapun, O. Dideberg, and T. Vernet.** 2004. The D,D-carboxypeptidase PBP3 organizes the division process of *Streptococcus pneumoniae*. Mol. Microbiol. **51:**1641–1648.
45. **Ng, W. L., K. M. Kazmierczak, and M. E. Winkler.** 2004. Defective cell wall synthesis in *Streptococcus pneumoniae* R6 depleted for the essential PcsB putative murein hydrolase or the VicR (YycF) response regulator. Mol. Microbiol. **53:**1161–1175.
46. **Ng, W. L., G. T. Robertson, K. M. Kazmierczak, J. Zhao, R. Gilmour, and M. E. Winkler.** 2003. Constitutive expression of PcsB suppresses the requirement for the essential VicR (YycF) response regulator in *Streptococcus pneumoniae* R6. Mol. Microbiol. **50:**1647–1663.
47. **Ng, W. L., H. C. Tsui, and M. E. Winkler.** 2005. Regulation of the *pspA* virulence factor and essential pcsB murein biosynthetic genes by the phosphorylated VicR (YycF) response regulator in *Streptococcus pneumoniae*. J. Bacteriol. **187:**7444–7459.
48. **Park, J. T., and T. Uehara.** 2008. How bacteria consume their own exoskeletons (turnover and recycling of cell wall peptidoglycan). Microbiol. Mol. Biol. Rev. **72:**211–227.
49. **Paton, J. C., and J. K. Morona.** 2006. *Streptococcus pneumoniae*: capsular polysaccharide, p. 242–252. *In* V. A. Fischetti, R. P. Novick, J. J. Ferretti, D. A. Portnoy, and J. I. Rood (ed.), Gram-positive pathogens. ASM Press, Washington, DC.
50. **Pereira, S. F., A. O. Henriques, M. G. Pinho, H. de Lencastre, and A. Tomasz.** 2007. Role of PBP1 in cell division of *Staphylococcus aureus*. J. Bacteriol. **189:**3525–3531.
51. **Pinho, M. G., and J. Errington.** 2005. Recruitment of penicillin-binding protein PBP2 to the division site of *Staphylococcus aureus* is dependent on its transpeptidation substrates. Mol. Microbiol. **55:**799–807.
52. **Pringle, J. R., A. E. Adams, D. G. Drubin, and B. K. Haarer.** 1991. Immunofluorescence methods for yeast. Methods Enzymol. **194:**565–602.
53. **Ramos-Montanez, S., H. C. Tsui, K. J. Wayne, J. L. Morris, L. E. Peters, F. Zhang, K. M. Kazmierczak, L. T. Sham, and M. E. Winkler.** 2008. Polymorphism and regulation of the *spxB* (pyruvate oxidase) virulence factor gene by a CBS-HotDog domain protein (SpxR) in serotype 2 *Streptococcus pneumoniae*. Mol. Microbiol. **67:**729–746.
54. **Rashel, M., J. Uchiyama, I. Takemura, H. Hoshiba, T. Ujihara, H. Takatsuji, K. Honke, and S. Matsuzaki.** 2008. Tail-associated structural protein gp61 of *Staphylococcus aureus* phage phi MR11 has bifunctional lytic activity. FEMS Microbiol. Lett. **284:**9–16.
55. **Reinscheid, D. J., K. Ehlert, G. S. Chhatwal, and B. J. Eikmanns.** 2003. Functional analysis of a PcsB-deficient mutant of group B streptococcus. FEMS Microbiol. Lett. **221:**73–79.
56. **Reinscheid, D. J., B. Gottschalk, A. Schubert, B. J. Eikmanns, and G. S. Chhatwal.** 2001. Identification and molecular analysis of PcsB, a protein required for cell wall separation of group B streptococcus. J. Bacteriol. **183:**1175–1183.
57. **Robertson, G. T., W. L. Ng, J. Foley, R. Gilmour, and M. E. Winkler.** 2002. Global transcriptional analysis of *clpP* mutations of type 2 *Streptococcus pneumoniae* and their effects on physiology and virulence. J. Bacteriol. **184:** 3508–3520.
58. **Sambrook, J., and D. W. Russell.** 2001. Molecular cloning: a laboratory manual, 3rd ed. Cold Spring Harbor Laboratory Press, Cold Spring Harbor, NY.
59. **Schuster, C., B. Dobrinski, and R. Hakenbeck.** 1990. Unusual septum formation in *Streptococcus pneumoniae* mutants with an alteration in the D,D-carboxypeptidase penicillin-binding protein 3. J. Bacteriol. **172:**6499–6505.
60. **Severin, A., A. M. Figueiredo, and A. Tomasz.** 1996. Separation of abnormal cell wall composition from penicillin resistance through genetic transformation of *Streptococcus pneumoniae*. J. Bacteriol. **178:**1788–1792.
61. **Severin, A., and A. Tomasz.** 1996. Naturally occurring peptidoglycan variants of *Streptococcus pneumoniae*. J. Bacteriol. **178:**168–174.
62. **Teng, F., M. Kawalec, G. M. Weinstock, W. Hryniewicz, and B. E. Murray.** 2003. An *Enterococcus faecium* secreted antigen, SagA, exhibits broad-spectrum binding to extracellular matrix proteins and appears essential for *E. faecium* growth. Infect. Immun. **71:**5033–5041.
63. **Tomasz, A., and W. Fischer.** 2006. The cell wall of *Streptococcus pneumoniae*, p. 230–240. *In* V. A. Fischetti, R. P. Novick, J. J. Ferretti, D. A. Portnoy, and J. I. Rood (ed.), Gram-positive pathogens, 2nd ed. ASM Press, Washington, DC.
64. **van den Ent, F., M. Leaver, F. Bendezu, J. Errington, P. de Boer, and J. Lowe.** 2006. Dimeric structure of the cell shape protein MreC and its functional implications. Mol. Microbiol. **62:**1631–1642.

65. **Viegas, S. C., P. Fernandez De Palencia, M. Amblar, C. M. Arraiano, and P. Lopez.** 2004. Development of an inducible system to control and easily monitor gene expression in *Lactococcus lactis*. Plasmid **51:**256–264.
66. **Vollmer, W., D. Blanot, and M. A. de Pedro.** 2008. Peptidoglycan structure and architecture. FEMS Microbiol. Rev. **32:**149–167.
67. **Vollmer, W., B. Joris, P. Charlier, and S. Foster.** 2008. Bacterial peptidoglycan (murein) hydrolases. FEMS Microbiol. Rev. **32:**259–286.
68. **Winkler, M. E., and J. A. Hoch.** 2008. Essentiality, bypass, and targeting of the YycFG (VicRK) two-component regulatory system in gram-positive bacteria. J. Bacteriol. **190:**2645–2648.
69. **Yother, J.** 2004. Capsules, p. 30–48. *In* E. I. Tuomanen, T. J. Mitchell, D. A. Morrison, and B. G. Spratt (ed.), The pneumococcus. ASM Press, Washington, DC.
70. **Young, K. D.** 2003. Bacterial shape. Mol. Microbiol. **49:**571–580.
71. **Zapun, A., T. Vernet, and M. G. Pinho.** 2008. The different shapes of cocci. FEMS Microbiol. Rev. **32:**345–360.